

## Semiconductor Nanocrystals

How to cite: *Angew. Chem. Int. Ed.* **2021**, 60, 9772–9788

International Edition: doi.org/10.1002/anie.202008395

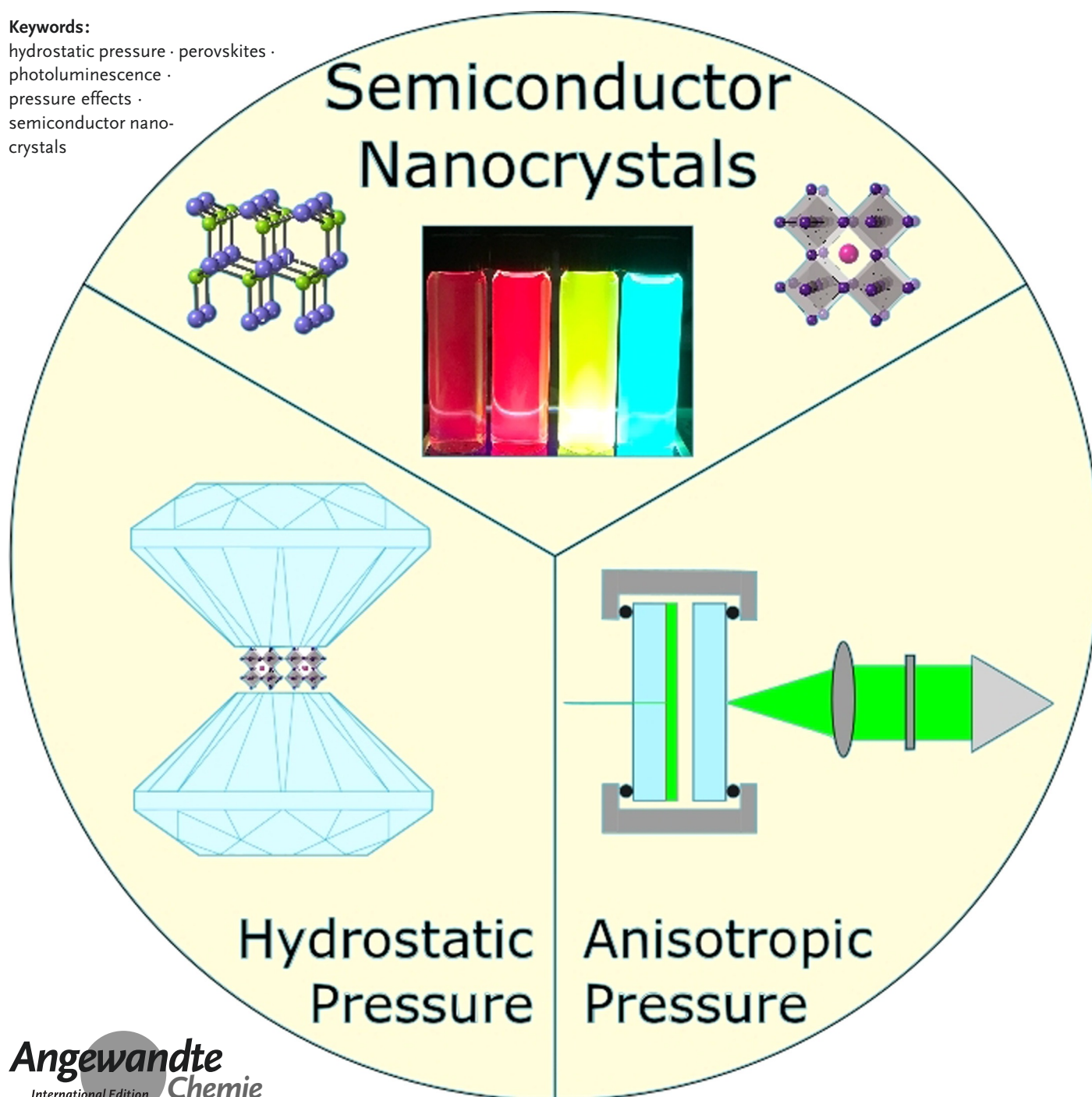
German Edition: doi.org/10.1002/ange.202008395

# Tailoring Optical Properties of Luminescent Semiconducting Nanocrystals through Hydrostatic, Anisotropic Static, and Dynamic Pressures

Gill M. Biesold, Shuang Liang, Blair Brettmann,\* Naresh Thadhani,\*  
Zhitao Kang,\* and Zhiqun Lin\*

**Keywords:**

hydrostatic pressure · perovskites ·  
photoluminescence ·  
pressure effects ·  
semiconductor nano-  
crystals



**L**uminescent semiconductor nanocrystals are a fascinating class of materials because of their size-dependent emissions. Numerous past studies have demonstrated that semiconductor nanoparticles with radii smaller than their Bohr radius experience quantum confinement and thus size-dependent emissions. Exerting pressure on these nanoparticles represents an additional, more dynamic, strategy to alter their size and shift their emission. The application of pressure results in the lattices becoming strained and the electronic structure altered. In this Minireview, colloidal semiconductor nanocrystals are first introduced. The effects of uniform hydrostatic pressure on the optical properties of metal halide perovskite ( $ABX_3$ ), II–VI, III–V, and IV–VI semiconductor nanocrystals are then examined. The optical properties of semiconductor nanocrystals under static and dynamic anisotropic pressure are then summarized. Finally, future research directions and applications utilizing the pressure-dependent optical properties of semiconductor nanocrystals are discussed.

## 1. Introduction

Pressure is a powerful thermodynamic variable that can unlock a multitude of unique characteristics. When applied to nanomaterials, it can lead to unique morphologies and properties.<sup>[1]</sup> For example, robust gold nanostructures have been produced by superfast dynamic compression,<sup>[2]</sup> and hydrostatic pressure has been used to convert silver nanoparticles into nanowires.<sup>[3]</sup> Although useful for many classes of materials, this Minireview will focus on how the application of pressure affects the optical properties of semiconductor nanocrystals (NCs).<sup>[4]</sup> Semiconductor NCs possess many properties that differ greatly from those seen in their bulk forms. Shrinking to the nanoscale has been shown to affect the band gap, radiative lifetime, melting temperature, and phase transition pressure of semiconducting materials.<sup>[5]</sup> Many of the differences in properties can be rationalized by quantum confinement, which occurs when the size of a NC is smaller than the Bohr radius of an exciton. This separates the energy levels of its electrons and effectively makes the band gap of a NC a function of its size.<sup>[5]</sup> NCs have been studied extensively in many environments (e.g. high temperature, acid, basic, etc.),<sup>[6–8]</sup> but high pressure is of particular interest.

The application of pressure has been shown to alter the crystal structure and electronic configuration of many bulk semiconducting materials.<sup>[9–13]</sup> The change in the electronic structure can be attributed to the resulting closer-packed structures and reduced interatomic distances.<sup>[14]</sup> Scrutinizing NCs under high pressure is of key importance, as it offers insight into how the electronic structure evolves when under the perturbation of two different forces: quantum confinement and pressure. Previous reviews on nanocrystals in high-pressure environments have focused on the pressure-induced crystallographic phase changes of conventional semiconductor NCs.<sup>[15–17]</sup> Although comprehensive when published, these reviews do not include perspectives on recently studied perovskite nanocrystals. It is also notable that past reviews


have also concentrated solely on the response of semiconductor NCs to hydrostatic pressure. This Minireview will discuss the following relevant topics: The general background of colloidal semiconductor nanocrystals (Section 1), the effects of uniform hydrostatic pressure on the optical properties of both metal halide perovskite and traditional semiconductor NCs (Section 2), the optical response of a variety of traditional semiconductor NCs to non-uniform (shock and anisotropic) pressures (Section 3), and future research directions and applications of the pressure-dependent optical properties of semiconductor NCs (Section 4).

## 2. Uniform Hydrostatic Pressure

Under hydrostatic pressure, all sides of an object experience uniform compression. The uniform distortion of semiconductor NCs results in many unique phenomena, as the following section will summarize. All studies outlined in this section were performed with a diamond anvil cell (DAC). Briefly, DAC tests involve the placement of a sample (i.e. semiconductor NCs) dispersed in a pressure media between two diamonds. The pressure media is needed to ensure the transfer of uniform pressure to all faces of the sample. Testing in DACs allow very high pressures (up to GPa) to be achieved. A representative image of a DAC is shown in the inset in Figure 1.

[\*] G. M. Biesold, S. Liang, Prof. B. Brettmann, Prof. N. Thadhani, Z. Kang, Prof. Z. Lin  
School of Materials Science and Engineering  
Georgia Institute of Technology  
Atlanta, Georgia 30332 (USA)  
E-mail: naresh.thadhani@mse.gatech.edu  
zhiquan.lin@mse.gatech.edu

Prof. B. Brettmann  
School of Chemical and Biomedical Engineering  
Georgia Institute of Technology  
Atlanta, Georgia 30332 (USA)  
E-mail: blair.brettmann@mse.gatech.edu  
Z. Kang  
Georgia Tech Research Institute  
Georgia Institute of Technology  
Atlanta, Georgia 30332 (USA)  
E-mail: Zhitao.kang@gtri.gatech.edu

 The ORCID identification number for some of the authors of this article can be found under: <https://doi.org/10.1002/anie.202008395>.

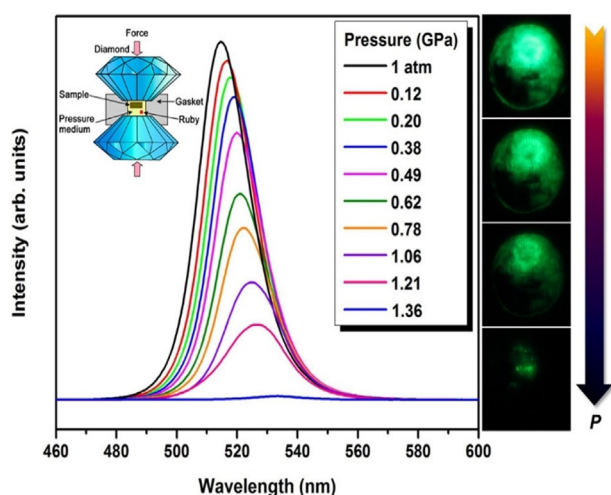


**Figure 1.** Evolution of the PL of CsPbBr<sub>3</sub> NCs as a function of applied pressure. The digital images (right panel) show the PL emission intensity at 1 atm, 0.49, 0.78, and 1.21 GPa. The inset (top left) is a graphical representation of a diamond anvil cell. Reproduced from Ref. [51] with permission, copyright 2017 American Chemical Society.

### 2.1. Effect of Hydrostatic Pressure on Metal Halide Perovskite Nanocrystals (MHP NCs)

Studies on the hydrostatic-pressure-dependent optical properties of a variety of metal-halide perovskites will be discussed below. Metal-halide perovskites (MHPs), which have the general formula ABX<sub>3</sub> [A = Cs<sup>+</sup>, CH<sub>3</sub>NH<sub>3</sub><sup>+</sup> (methylammonium, MA), HC(NH<sub>3</sub>)<sub>2</sub><sup>2+</sup> (formamidinium, FA), etc.; B = Pb<sup>2+</sup>, Sn<sup>2+</sup>, etc.; and X = Cl, Br, or I], have been widely studied because of their tremendous potential for use in many optoelectronic applications, including solar cells,<sup>[18–21]</sup>

LEDs,<sup>[22–26]</sup> photodetectors,<sup>[27,28]</sup> and scintillators.<sup>[29]</sup> The exceptional optical performance of MHPs can be attributed to their strong optical absorption,<sup>[30,31]</sup> low exciton binding energy,<sup>[32]</sup> long exciton diffusion lengths,<sup>[33]</sup> high carrier mobility,<sup>[34,35]</sup> defect tolerance,<sup>[36–38]</sup> and facile synthesis.<sup>[35,39]</sup> Lead-halide perovskites (LHPs) are a class of MHPs that have shown great promise as a result of the abovementioned unique properties and their relatively high stability.<sup>[40]</sup> LHP NCs are of particular interest because of their extremely bright and narrow photoluminescence (PL) band and the ease of tuning their emission wavelengths by tuning both the halide composition and the size of the NCs.<sup>[41–47]</sup> The following subsections will outline how the application of hydrostatic pressure alters the optical properties of a variety of LHP NCs.

#### 2.1.1. All-Inorganic CsPbX<sub>3</sub> Perovskites

Cs<sup>+</sup> is a commonly used A-site cation in all-inorganic LHP NCs because its large ionic radius ( $R_A = 1.88 \text{ \AA}$ ) allows the formation of a stable perovskite phase, as determined by the Goldschmidt tolerance factor.<sup>[48]</sup> CsPbBr<sub>3</sub> NCs have been shown to possess a near-unity photoluminescence quantum yield (PLQY), narrow (i.e. 86 meV) full width at half max (FWHM), and superior stability to both CsPbI<sub>3</sub> and CsPbCl<sub>3</sub>.<sup>[49,50]</sup> When subjected to hydrostatic pressures up to about 1.4 GPa, the PL spectra of CsPbBr<sub>3</sub> NCs was red-shifted, widened, and decreased in intensity until ca. 1.3 GPa, at which pressure the PL was sharply quenched (Figure 1).<sup>[51]</sup> The authors attributed the discontinuity to an isostructural phase transformation of the *Pbnm* space group.<sup>[51]</sup> First-principle calculations suggested that the shift in the emission and the phase change were due to pressure-induced variations of the Br–Pb bond lengths and shrinkage of the Pb–Br–Pb bond angles within the lead bromide octahedra.<sup>[51]</sup> Interest-



Gill M. Biesold is a PhD student at the Materials Science and Engineering department at Georgia Institute of Technology. He received his B.S. in Materials Science and Engineering from Clemson University in 2017. His current research is focused on quantum dots and their potential applications in lasing and sensing.



Blair Brettmann is a Professor of Chemical and Biomolecular Engineering and Materials Science and Engineering at Georgia Tech. She received her Ph.D. in Chemical Engineering at the Massachusetts Institute of Technology in 2012. Her research focuses on linking polymer and particle molecular-scale phenomena to processing and multicomponent complex mixtures to enable rapid and science-driven formulation and product development.



Shuang Liang is a PhD student in Dr. Zhiqun Lin's group at the Georgia Institute of Technology since 2017. He received his B.E. in Chemical Engineering from Southeast University, China, in 2017. His current research is focused on the synthesis and application of functional semiconducting nanomaterials, block copolymers, and polymer-based nanocomposites.



Naresh Thadhani is Professor and Chair of the School of Materials Science and Engineering (MSE) at Georgia Tech (GT). He received his Ph.D. from New Mexico Tech, in Metallurgical Engineering in 1984. His research is focused on the fundamental mechanisms of physical, chemical, and mechanical changes under high-pressure shock compression, and the deformation and fracture response of metals, ceramics, polymers, and composites when subjected to impact and high-strain-rate loading.



ingly, unlike NCs, the emission of bulk CsPbBr<sub>3</sub> was not found to monotonically red-shift under pressure.<sup>[52]</sup> Under hydrostatic pressure, the PL of bulk CsPbBr<sub>3</sub> was observed to red-shift until about 1.0 GPa (at which pressure it experienced a phase transformation) and then blue-shift until the emission was quenched. No rationale was given for the divergence in properties of the bulk and nanocrystalline CsPbBr<sub>3</sub>. To elucidate the effect that the size of the NCs has on pressure-dependent PL, CsPbBr<sub>3</sub> NCs with sizes ranging from 5.7 to 10.9 nm were examined at pressures up to 2.0 GPa.<sup>[53]</sup> The PL of all the NCs was found to red-shift with pressure, with larger NCs generally displaying a greater red-shift. The pressure coefficients  $\alpha$  ( $\alpha = dE/dp$ , emission energy shift per applied pressure [meV GPa<sup>-1</sup>]) of the NCs ranged from -15 meV GPa<sup>-1</sup> (for 6 nm NCs) to -45 meV GPa<sup>-1</sup> (for 8 nm NCs). The bandgap pressure coefficient is a convenient metric that represents the change in the optical band gap of a material as a function of applied pressure. Note that the largest NC (11 nm) was observed to possess an  $\alpha$  value of -40 meV GPa<sup>-1</sup>, the only sample reversing the trend. The size dependence of the pressure coefficient was ascribed to the fact that larger NCs have less surface tension than smaller NCs, which ensured less initial overlap of the Pb 6s and Br 4p orbitals.

The pressure-dependent PL of CsPbBr<sub>3</sub> NCs with Ruddlesden-Popper (RP) faults was also examined.<sup>[54]</sup> Ruddlesden-Popper faults are caused by the formation of AX layers between two ABX<sub>3</sub> perovskite domains, which results in a shift of half the unit cell of one of the ABX<sub>3</sub> domains relative to the other. NCs with RP faults displayed vastly different pressure-dependent PL behavior than pristine CsPbBr<sub>3</sub>. The PL intensity of NCs with RP faults initially decreased as the pressure increased, spiked at 1 GPa beyond that observed at ambient pressure, and then continued to decrease until quenching at 1.6 GPa. Interestingly, the PL

peak position was found to red-shift until 0.8 GPa and then blue-shift until quenching at 1.6 GPa. DFT calculations attributed these unique PL behaviors to the presence of the RP faults and the orthorhombic to monoclinic structural phase transition at 0.74 GPa. CsPbBr<sub>3</sub> NCs were also studied by cycling applied hydrostatic pressures from 0 to 17.5 GPa.<sup>[55]</sup> It was found that pressures in excess of 5.1 GPa led to ligand detachment, direct facet-to-facet contact, and the fusion of CsPbBr<sub>3</sub> NCs into 2D nanoplatelets of uniform thickness. These new nanoplatelets exhibited a single cubic structure, a 1.6-fold enhanced PL, and a longer emission lifetime than the initial NCs. The enhanced PL properties were attributed to the increased crystallinity and fewer defects/surface trap states in the nanoplatelets. The high-pressure transformation of NCs to nanoplatelets was not found to be reversible (unlike the reversible phase changes seen at 1.2 GPa).<sup>[51,52,55]</sup>

Although less stable than CsPbBr<sub>3</sub>, CsPbI<sub>3</sub> NCs possess many favorable optical properties and have also been widely studied. The PL of CsPbI<sub>3</sub> was explored at hydrostatic pressures up to 3.4 GPa.<sup>[56]</sup> The CsPbI<sub>3</sub> NCs exhibited an initial red-shift in their PL up to 0.38 GPa, at which the NCs transformed from a cubic to an orthorhombic phase. Beyond 0.38 GPa, a consistent blue-shift in the emission was seen until the PL was quenched by pressure-induced amorphization at 3.43 GPa (Figure 2a).<sup>[56]</sup> Theoretical calculations suggested that the differing optical responses were due to the shrinking of the Pb-I bonds lengths and variations in the Pb-I-Pb bond angles (Figure 3).<sup>[56]</sup> CsPbI<sub>3</sub> NCs were observed to transform from emissive to non-emissive phases at a lower pressure than their bulk counterpart (3.43 GPa for NCs, 3.9 GPa for bulk).<sup>[57]</sup> In a separate study of CsPbI<sub>3</sub> NCs under hydrostatic pressures up to 2.5 GPa, the PL was observed to initially red-shift up to 0.33 GPa and then consistently blue-shift until the test concluded (Figure 2b).<sup>[58]</sup> The red- and blue-shifting phenomena of CsPbI<sub>3</sub> NCs was rationalized by noting that different modes of crystal compression have different effects on the valence band maxima (VBM) and conduction band minima (CBM; Figure 3).<sup>[56,58]</sup> Initially, when pressure is applied, the octahedra tilt, which destabilizes the CBM and leads to an increase and concomitant blue-shift of the PL. The further application of pressure causes compression of the octahedra, which greatly destabilizes the VBM and results in an overall narrowing of the band gap. Eventually, the pressure is great enough to trigger amorphization of the NCs, which was found to quench the emission.<sup>[56,58]</sup> The divergence in the pressure-dependent PL behaviors of CsPbBr<sub>3</sub> (monotonic blue-shift) and CsPbI<sub>3</sub> (slight blue-shift, followed by a consistent red-shift) was attributed to the differences in the ionic radii of bromide and iodide, with the larger radius of iodide changing the dominant mode of deformation at a much lower pressure.<sup>[58]</sup>

The PL of 2.4% Mn<sup>2+</sup>-doped CsPbCl<sub>3</sub> NCs was also examined at pressures ranging from ambient to 7.1 GPa.<sup>[59]</sup> The NCs displayed an initial red-shift from ambient pressure to 1.7 GPa, followed by a continuous blue-shift up to 4.5 GPa. The transition from red-shifting to blue-shifting at 1.7 GPa was attributed to an underlying pressure-induced structural phase transition of the NCs. Notably, in situ XRD studies suggested that a transition from cubic to orthorhombic began



Zhitao Kang received his Ph.D. at the School of Materials Science and Engineering at Georgia Institute of Technology in 2006. He is a Principal Research Engineer at Georgia Tech Research Institute and an Adjunct Professor in School of Materials Science and Engineering at Georgia Institute of Technology. His current research focuses on the development of luminescence materials, growth and processing of thin films, and fabrication of photonic/optoelectronic devices.



Zhiqun Lin is a Professor in the School of Materials Science and Engineering at the Georgia Institute of Technology. He received his Ph.D. in Polymer Science and Engineering from the University of Massachusetts, Amherst in 2002. His research interests include functional nanocrystals, polymer-based nanocomposites, block copolymers, conjugated polymers, solar cells, batteries, photocatalysis, electrocatalysis, thermoelectrics, hierarchically structured and assembled materials, and surface and interfacial properties.

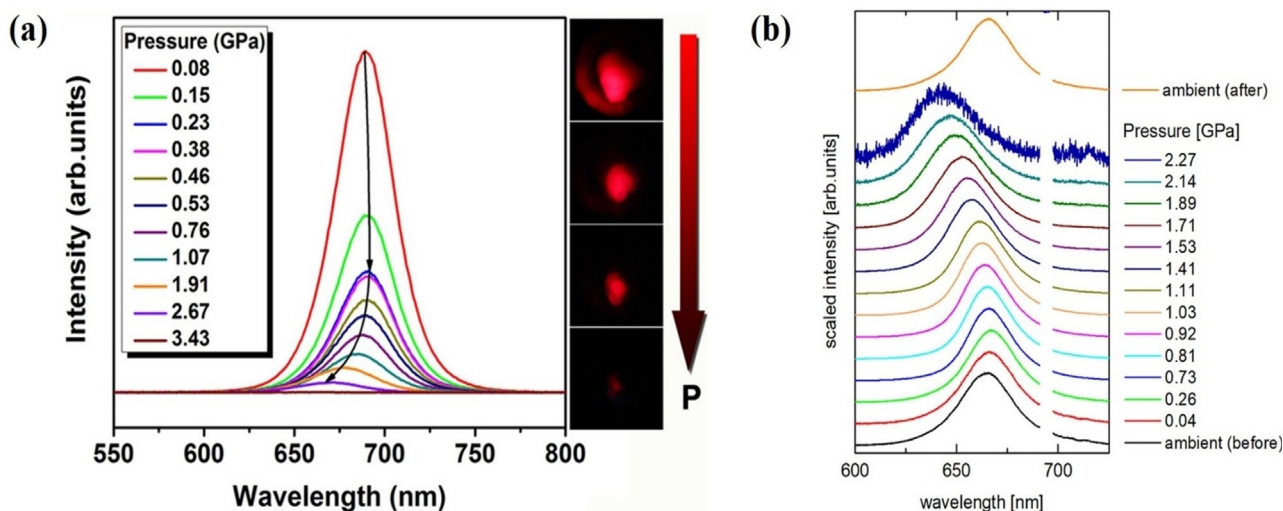


**Figure 2.** a) Evolution of the PL of CsPbI<sub>3</sub> NCs as a function of applied pressure. The digital images show the PL emission at 1 atm, 0.38 GPa, 1.07 GPa, and 3.43 GPa. The subtle red-shift in the emission at low pressures prior to the consistent blue-shift beyond 0.38 GPa is evident. The initial red-shift was attributed to a structure change of  $\alpha$ -CsPbI<sub>3</sub>. Reproduced from Ref. [56] with permission, copyright 2019 American Chemical Society. b) PL evolution of CsPbI<sub>3</sub> NCs under various hydrostatic pressures. The red-shift at lower pressures and the eventual blue-shift at higher pressures are clearly evident. Reproduced from Ref. [58] with permission, copyright 2018 American Chemical Society.

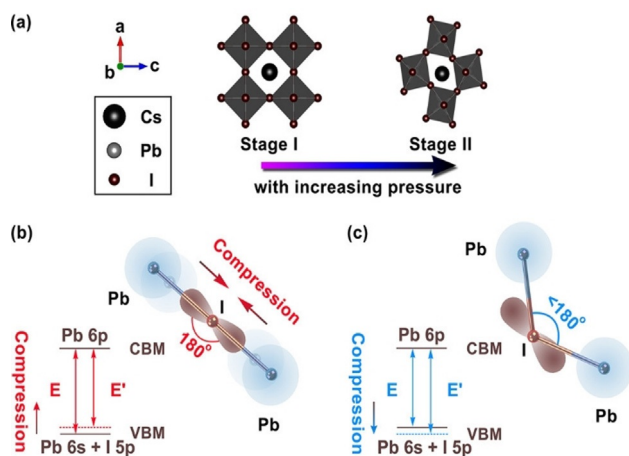


**Figure 3.** a) Schematic models of polyhedral views of cubic and orthorhombic CsPbI<sub>3</sub> perovskites under high pressure. b,c) Schematic illustrations of the changes in the band gap governed by the Pb-I-Pb bond angle within the PbI<sub>6</sub> octahedral framework before (b) and after (c) structural phase transition. Reproduced from Ref. [56] with permission, copyright 2019 American Chemical Society.

at 1.1 GPa, which does not correlate with the pressure where the PL-shifting behavior changed. CsPb<sub>x</sub>Mn<sub>1-x</sub>Cl<sub>3</sub> NCs were also observed to exhibit pressure-induced emission enhancement (PIEE).<sup>[60]</sup> The NCs were found to have two emission bands, one centered on  $\lambda = 406$  nm (from CsPb<sub>x</sub>Mn<sub>1-x</sub>Cl<sub>3</sub>) and the other at  $\lambda = 608$  nm (from Mn). Under pressures ranging from 0.17 to 1.23 GPa, the CsPb<sub>x</sub>Mn<sub>1-x</sub>Cl<sub>3</sub> and Mn bands both red-shifted, from  $\lambda = 406$  to 411 nm and from  $\lambda = 608$  to 638 nm, respectively. The intensity of the two bands was found to decrease as the pressure increased, but at 1.41 GPa, the Mn band was observed to undergo PIEE. This PIEE was attributed to the isostructural transformation-induced enhancement of energy release from  $^4T_1$  to  $^6A_1$  of the Mn atom.

### 2.1.2. Other All-Inorganic Perovskite-Like Materials

The perovskite family of materials extends beyond the simple ABX<sub>3</sub> structure. In another study, non-fluorescent zero-dimensional Cs<sub>4</sub>PbBr<sub>6</sub> perovskite-like NCs displayed emission after application of 3.01 GPa pressure, with further compression resulting in a significant increase in the emission.<sup>[61]</sup> Experimental and theoretical analysis of this phenomenon attributed the pressure-induced emission to the formation of self-trapped excitons, which are more favorably formed when the [PbBr<sub>6</sub>]<sup>4-</sup> octahedral motifs are distorted.<sup>[61,62]</sup> The pressure-dependent optical properties of Cs<sub>2</sub>AgBiBr<sub>6</sub> NCs were also explored.<sup>[63]</sup> The absorption of Cs<sub>2</sub>AgBiBr<sub>6</sub> NCs was seen to red-shift from ambient pressure to 2.0 GPa, and then blue-shift from 2.0 to 13.0 GPa. Notably, a distinct “blue jump” was seen at 4.5 GPa. First principles calculations ascribed these phenomena to the orbital interactions that occurred as a result of the pressure-induced tilting and distortion of the [AgBr<sub>6</sub>]<sup>5-</sup> and [BiBr<sub>6</sub>]<sup>3-</sup> octahedra.

### 2.1.3. Organolead Halide Perovskite

Organolead halide perovskites have small organic cations such as methylammonium (MA) and formamidinium (FA), rather than inorganic cesium ions, occupying the A site. Studies on the pressure-dependent emission of organolead halide perovskite NCs are limited. The PL of methylammonium lead iodide (MAPbBr<sub>3</sub>) NCs was studied at pressures up to 11 GPa.<sup>[64]</sup> The PL was seen to initially red-shift up to about 1 GPa, and then blue-shift until amorphization at approximately 3 GPa. In situ XRD data showed that as the pressure increased from ambient, the crystal structure of MAPbBr<sub>3</sub> NCs transitioned from cubic  $Pm\bar{3}m$  to cubic  $Im\bar{3}$  and from cubic  $Im\bar{3}$  to orthorhombic  $Pnma$  at pressures of 0.99 GPa and 2.41 GPa, respectively. The red-shift in going from ambient

pressure to 0.99 GPa (the  $Pm\bar{3}m$  range) was attributed to an increase in the VBM as a result of enhanced interaction of the Pbs and Brp orbitals through contraction of the Pb–Br bond. Further application of pressure (from 0.99 GPa to 3 GPa) was found to decrease the Pb–Br–Pb bond angle, which widened the band gap.<sup>[56,58,64]</sup> These results are in agreement with those of bulk MAPbBr<sub>3</sub> perovskite, which follows the same trend of red-shifting in the  $Pm\bar{3}m$  range and blue-shifting through the  $Im\bar{3}$  and  $Pnma$  structures.<sup>[65]</sup> Although the trends are identical, the bulk samples were seen to alter at lower pressures, with all phase transformations completed by 2 GPa. In both the bulk and NC cases, the shifts in the PL are consistent with the pressure-induced phase changes. The pressure-dependent PL behavior of the butylammonium lead halide [(C<sub>4</sub>H<sub>9</sub>NH<sub>3</sub>)<sub>2</sub>PbI<sub>4</sub>] hybrid perovskite flakes with 2D morphology was examined from 0 to 10 GPa.<sup>[66]</sup> From 0 to 0.14 GPa, the PL slightly red-shifted from  $\lambda = 524$  to 527 nm (band I), and at 0.14 GPa, a second band at  $\lambda = 503$  nm was observed, which suggested the emergence of a second phase (band II). As pressure continued to increase, band II was found to consistently red-shift. At 1.4 GPa, another band appeared at  $\lambda \approx 540$  nm, which indicated the formation of a third phase (band III). As the pressure continued to increase, band III became the dominant emission and continued to red-shift

until quenching at 10 GPa. The three distinct emission bands were ascribed to the pressure-induced phase transitions of *Pbca* (1a) to *Pbca* (1b) (at 0.14 GPa) and *Pbca* (1b) to *P2<sub>1</sub>/a* (at 1.4 GPa).

The PL energy of formamidinium lead iodide (FAPbI<sub>3</sub>) NCs was found to blue-shift from 1.44 to 2.17 eV under applied pressures ranging from 0 to 13.4 GPa.<sup>[67]</sup> It was shown that, similar to MAPbBr<sub>3</sub>, FAPbI<sub>3</sub> undergoes a phase transition from cubic  $Pm\bar{3}m$  to cubic  $Im\bar{3}$ , although the FAPbI<sub>3</sub> transformation occurred at a lower pressure of 0.6 GPa. It was observed that further pressure increases led to gradual amorphization, with full amorphization occurring at 7.1 GPa. Unlike MAPbX<sub>3</sub> perovskites, an orthorhombic *Pnma* phase of FAPbI<sub>3</sub> was not seen. A single pressure-driven phase transformation has also been found in bulk FAPbI<sub>3</sub> (from cubic  $Pm\bar{3}m$  to cubic  $Im\bar{3}$ ) before amorphization.<sup>[68]</sup> As seen in Figure 4, the PL of the FAPbI<sub>3</sub> NCs consistently red-shifted at pressures from ambient up to 2.3 GPa, and then abruptly blue-shifted, which was ascribed to the onset of amorphization.<sup>[67]</sup> This phenomenon was similar to that of bulk FAPbI<sub>3</sub>, the PL of which has been shown to red-shift up to 2.1 GPa.<sup>[68,69]</sup> DFT calculations determined that both the red-shift and blue-shift observed in the pressure-dependent PL of FAPbI<sub>3</sub> were due to the

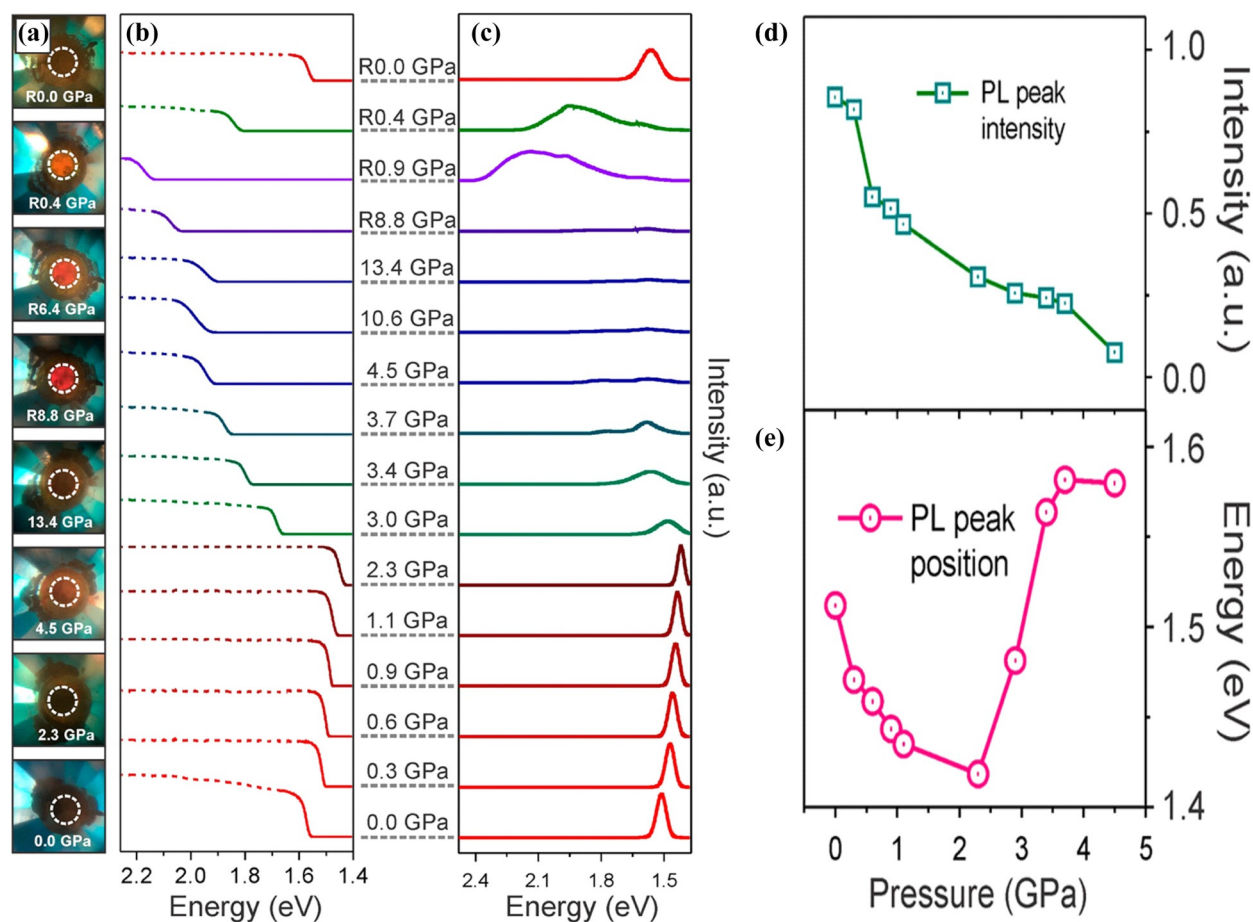


**Figure 4.** a) Images of FAPbI<sub>3</sub> NCs under increasing pressure. b) Absorption and c) PL spectral evolutions of FAPbI<sub>3</sub> NCs with the pressure increasing from 0 to 13.4 GPa. d) PL band intensity and e) PL band position as a function of increased pressure. Reproduced from Ref. [67] with permission, copyright 2018 American Chemical Society.



structural behavior of the  $[\text{PbI}_6]^{4-}$  octahedral subunits.<sup>[67]</sup> Calculations suggest that below 0.6 GPa (the transition pressure from cubic  $Pm\bar{3}m$  to cubic  $Im\bar{3}$ ) homogeneous contraction of the octahedra shortened the Pb–I bonds which resulted in overlap of two p orbitals and narrowed the band gap. After phase transition to cubic  $Im\bar{3}$ , a further increased pressure altered the Pb–I–Pb bond angle, thereby altering the symmetry between the Pb 6p and I 5p orbitals, and resulting in a narrowed band gap. As the NCs approach amorphization above 3.0 GPa, the band gap as expected increases. These results are consistent with other studies that have observed a decreasing intensity of the PL band as a function of increasing pressure (Figure 4D).

## 2.2. Effect of Hydrostatic Pressure on Conventional Semiconductor Nanocrystals

In the following section, the dependence of the optical properties of conventional II–VI, III–V, and IV–VI NCs, also known as quantum dots (QDs), on hydrostatic pressure will be examined.

### 2.2.1. II–VI Semiconductor NCs

CdSe NCs are a well-studied class of nanomaterials.<sup>[70–72]</sup> They exhibit good stability, PLQY, and size monodispersity. The dependence of the PL of 2.4 nm CdSe NCs on the hydrostatic pressure was investigated at pressures up to 5.2 GPa.<sup>[73]</sup> As illustrated in Figure 5, the PL energy was observed to linearly increase with pressure, thereby yielding a band gap pressure coefficient ( $\alpha$ ) of 27 meV GPa<sup>−1</sup> (PL band was ca. 2.1 eV at 0 GPa and ca. 2.25 eV at 5.2 GPa).<sup>[73]</sup> Achieving a consistent value for the band gap pressure coefficient ( $\alpha$ ) has proven elusive, as other studies on the hydrostatic-pressure-dependence of the PL of CdSe NCs have yielded the following values for  $\alpha$ : 27 meV GPa<sup>−1</sup>,<sup>[73–75]</sup> 45 meV GPa<sup>−1</sup>,<sup>[76]</sup> and 82 meV GPa<sup>−1</sup>.<sup>[77]</sup> The reported  $\alpha$  value of bulk CdSe varies according to the method used to attain it (i.e. 37 meV GPa<sup>−1</sup> (absorption),<sup>[13]</sup> 43.1 meV GPa<sup>−1</sup> (photo-modulated transmission),<sup>[78]</sup> and 58 meV GPa<sup>−1</sup> (PL).<sup>[79]</sup> In an effort to identify a more cohesive value of  $\alpha$ , density functional theory (DFT) was utilized to theoretically calculate the deformation potential  $\alpha_v$  of CdSe NCs.<sup>[14]</sup> The deformation potential  $\alpha_v$  (the effective potential experienced by free electrons in a semiconductor resulting from deformation of the lattice), was used as a proxy for  $\alpha$ , because the local density approximation employed in DFT cannot accurately calculate  $\alpha$ . It was found that the amplitude of  $\alpha_v$  increased as the size of the NCs decreased, with the  $\alpha_v$  value for a 1.7 nm CdSe NC being 20 % greater than that of the bulk. The value of  $\alpha_v$  for 4 nm NCs (the size of many experimentally studied NCs) was only calculated to increase by 3 %, which does not explain the diverging values of  $\alpha$ . The inability to determine an accurate value is a crucially important for understanding exactly how much pressure affects the PL properties of CdSe NCs.

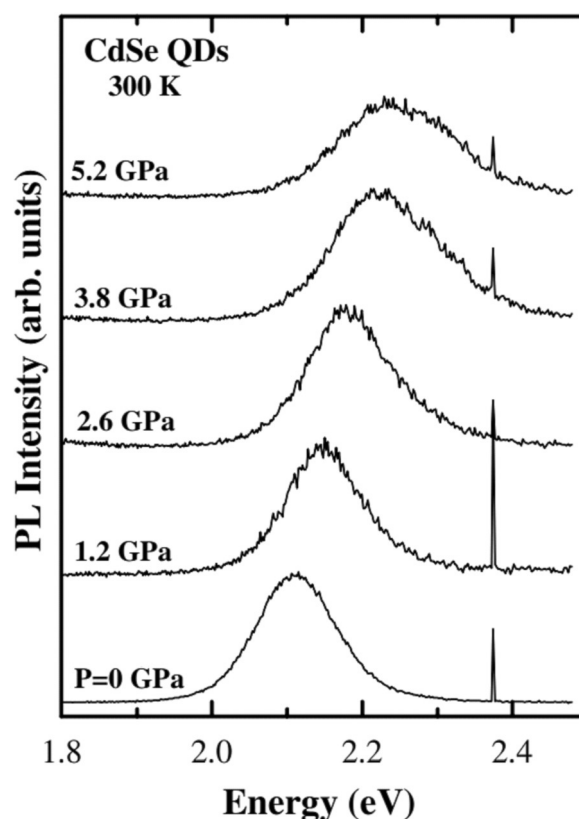


**Figure 5.** Pressure-dependence of the PL spectra of CdSe NCs under various hydrostatic pressures. Reproduced from Ref. [73] with permission, copyright 2001 Institute of Physics Publishing.

CdSe NCs have been observed to transform from wurtzite to rock salt phases at pressures between 3.6 and 4.9 GPa.<sup>[80]</sup> The recorded phase transition pressures are greater for NCs than for bulk CdSe, which ranges from 2.5 to 3.5 GPa.<sup>[79,81]</sup> Interestingly, no sharp discontinuities in the PL evolution of CdSe NCs were observed at pressures ranging from ambient to 5.2 GPa, even though the pressures were sufficient for the wurtzite to rock transformation (as seen in Figure 5).<sup>[73,80]</sup> The absorption of CdSe NCs was monitored during the transition from direct-band-gap wurtzite to indirect-band-gap rock salt to further elucidate the effect of phase change on optical properties.<sup>[82]</sup> Intriguingly, there was a sharp difference in the absorption spectra of the wurtzite phase (0.1 GPa) and rock salt phase (8.5 GPa), which suggests that discontinuities in the PL emission might occur at higher pressures than were tested.<sup>[73]</sup>

The PL properties of both CdSe NCs and CdSe NC arrays were examined at pressures ranging from 0 to 7 MPa to better understand the interaction of multiple NCs under pressure.<sup>[74]</sup> The emission and absorption of both CdSe NCs and CdSe NC arrays were found to blue-shift consistently with applied pressure. The PL shift of arrays and individual NCs was approximately the same, ranging from 2.25 eV (no pressure) to 2.40 eV (7 GPa). It is interesting to note that a significant Stokes shift was observed, which was attributed to the increased vibrational relaxation caused by the movement of nuclei in the excited state. The expected transition from the

rock salt structure occurs above 6.5 MPa, as previously noted.<sup>[80,81]</sup> The similar PL shifts seen for arrays and individual NCs suggest that little to no coupling occurs in the arrays.

CdTe NCs are another II–VI semiconductor that has been explored for hydrostatic-pressure-dependent PL. In its bulk form, the emission band energy of CdTe has been shown to blue-shift from 1.5 eV (ambient conditions) to near 1.8 eV at an applied pressure of 3 GPa.<sup>[79]</sup> The hydrostatic-pressure-dependent PL of three different diameter water-soluble CdTe NCs was evaluated at pressures from ambient to about 7 GPa.<sup>[83]</sup> The PL emissions of all sizes of the CdTe NCs were blue-shifted, decreased in intensity, and widened upon the application of pressure (Figure 6). The NC size was also found to directly affect the phase transition pressure from zinc-blende to rock salt. The phase transitions of CdTe NCs with diameters of 5.1 nm, 3.4 nm, and 2.3 nm were completed at pressures of 7.6 GPa, 6.3 GPa, and 5.4 GPa, respectively. This behavior is starkly different from that of CdSe NCs, the phase transition pressure of which was found to increase with decreasing size.<sup>[81]</sup> This was assigned to different surface conditions, as a result of very different ligands. Thiol-capped CdTe NCs were examined at hydrostatic pressures up to 37.0 GPa.<sup>[84]</sup> In this investigation, solution-phase CdTe NCs were observed to transform from a cinnabar to a rock salt phase at 5.8 GPa, which is much higher than that of either bulk CdTe (3.8 GPa) or solid CdTe NCs. The increased stability was ascribed to the possible shape change in the phase transition or to inhomogeneous strains in nanoparticle solutions.<sup>[84]</sup>

DFT calculations were used to investigate the effects of pressure, size, and surface ligands on the optical properties of CdS NCs.<sup>[85]</sup> This study examined two sizes of CdS NCs (Cd<sub>10</sub>S<sub>4</sub> and Cd<sub>32</sub>S<sub>14</sub>) with two different terminal groups as ligands (phenyl and hydrogen) at pressures ranging from 0 to 15 GPa. Both sizes of NCs terminated by phenyl groups were found to consistently red-shift their emission, with the larger NCs doing so to a greater degree. The larger H-terminated NCs exhibited a slight blue-shift up to 5 GPa, where it red-

shifted, and the small H-terminated NCs had a relatively unchanged PL. It was suggested that the different behaviors were due to two competing processes, that is, a bulk-like tendency to blue-shift with increasing pressure and ligand-induced distortions and hybridization of the frontier orbitals.

Semiconductor NCs can also be an alloyed mixture of more than two components. The pressure-dependent PL of 5.5 nm wurtzite phase CdZnSe alloy QDs was compared to that of 3.5 nm CdSe NCs.<sup>[86]</sup> Similar to other CdSe NCs, it was found that pressure led to a blue-shift of the emission, with the pressure coefficients  $\alpha$  for CdZnSe and CdSe NCs being 35.4 meV GPa<sup>−1</sup> and 28.4 meV GPa<sup>−1</sup>, respectively. The relatively larger value for the alloyed NC was credited to the alloying effect. Alloying was found to strengthen the anion–cation s–s orbital coupling and weaken the p–d orbital coupling, which has been shown to increase and decrease  $\alpha$ , respectively.<sup>[87,88]</sup> Core/shell CdSe/CdS NCs with 1, 2, 3, and 4 monolayer (ML) thick CdS shells were investigated to elucidate the effect of shell thickness on the pressure-dependent PL.<sup>[89]</sup> The application of pressure was found to blue-shift the emission of all four samples with different shell thicknesses. Interestingly, samples with thicker shells maintained their emission at higher pressures than those with thinner shells (1 and 4 ML samples were quenched at 7.67 and 9.02 GPa, respectively). The changes in the optical properties were attributed to a pressure-induced transition from a quasi-type II to type I core/shell structure. It has been shown using first principles calculations that strain (such as that caused from high pressure) has a large effect on the band offsets of core/shell NCs.<sup>[90]</sup> This theoretical calculation verified that pressure plays a role in both type I and type II band gap NCs, with CdSe/CdS and CdSe/CdTe as the examples. CdS<sub>1−x</sub>Se<sub>x</sub> (0.4 <  $x$  ≤ 1) NCs were embedded into a glass matrix and subjected to hydrostatic pressures up to 0.4 GPa.<sup>[91]</sup> The emissions of all samples were found to blue-shift, with band gap pressure coefficients ranging from 0.034 to 0.070 eV GPa<sup>−1</sup>, and displaying no dependence on NC size or composition. The hydrostatic-pressure-dependence of the PL of unalloyed ZnO and alloyed Mg<sub>0.15</sub>Zn<sub>0.85</sub>O NCs were examined.<sup>[92]</sup> The PL of Mg<sub>0.15</sub>Zn<sub>0.85</sub>O NCs was found to blue-shift as the pressure increased to a maximum of 7 GPa. The band gap pressure coefficient  $\alpha$  for ZnO and Mg<sub>0.15</sub>Zn<sub>0.85</sub>O NCs were found to be 23.6 and 27.1 meV GPa<sup>−1</sup>, respectively. It was rationalized that the alloyed sample had a larger  $\alpha$  value because of the same alloying effects noted above.<sup>[87,88]</sup>

The PL evolution from CdSe/ZnS core/shell NCs in an Epo-Tek 305 epoxy resin cuboid was investigated under lower pressure.<sup>[93]</sup> An NC/epoxy cuboid was placed in a load frame with a custom apparatus that constrained lateral expansion of the sample. Pressure was then applied to the sample, and the PL was measured. This study focused on lower pressure dependence, with a maximum pressure of only 69 MPa. The NC emission intensity decreased as the pressure was increased, but no shift in the emission wavelength was detected. A control experiment with CdSe/ZnS core/shell NCs in a DAC under hydrostatic pressures ranging from 0 to 69 MPa showed no decrease in intensity, which led to the conclusion that the observed emission was not due to pressure but rather interactions between the NCs and the solid matrix. The PL of

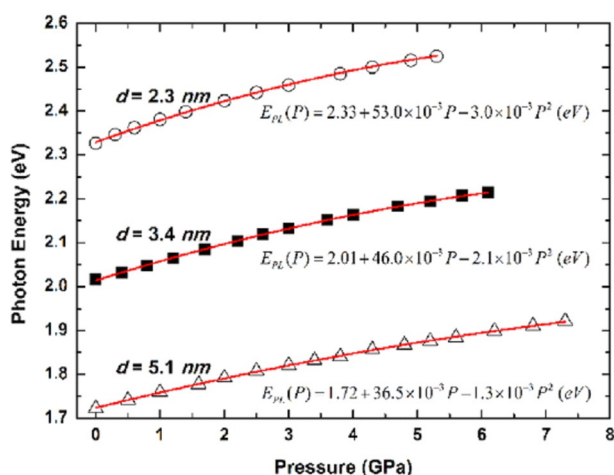


**Figure 6.** Pressure-dependent emission peaks of 3-mercaptopropionic acid capped CdTe NCs with diameters of 2.3, 3.4, and 5.1 nm. Reproduced from Ref. [83] with permission, copyright the 2015 International Society for Optics and Photonics.



core/shell CdSe/ZnS NCs was also investigated at higher pressures, ranging from 0 to 7.0 GPa.<sup>[94]</sup> The PL was consistently observed to blue-shift as pressure was applied, although the shifting occurred in two distinct regions. From 0 to 3.48 GPa, the band gap pressure coefficient was found to be  $31 \text{ meV GPa}^{-1}$ , and beyond 3.48 GPa the pressure coefficient decreased to  $9 \text{ meV GPa}^{-1}$ . The lower pressure coefficient beyond the 3.48 GPa critical point was attributed to the pressure-induced increase of the bulk modulus. Above 3.48 GPa, the interdot coupling was also increased, which was verified by an increased PL decay time in the higher-pressure regime.

### 2.2.2. III–V Semiconductor NCs

A variety of III–V semiconductor NCs have also been explored for their hydrostatic-pressure-dependent PL. The PL of self-assembled InAs NCs in a GaAs matrix was examined in a magnetic field up to 23 T and hydrostatic pressures up to 0.8 GPa.<sup>[95]</sup> The emission of the NCs was found to blue-shift, with a pressure coefficient  $\alpha$  of  $91 \text{ meV GPa}^{-1}$ . InAs NCs have been mixed with GaAs to create alloyed NCs. The PL of large, ( $D = 78 \text{ nm}$ ) self-assembled, long-wavelength InAs/GaAs NCs was examined under hydrostatic pressures up to 9 GPa at 15 K.<sup>[96]</sup> Two photoemissions were noted, one from the ground state and the other from the first excited state, with pressure coefficients  $\alpha$  of 69 and  $72 \text{ meV GPa}^{-1}$ , respectively. The band gap of InAs/GaAs NCs was seen to increase from 1.1 eV to about 1.6 eV at an applied pressure of 8 GPa. The ground exciton energy pressure coefficients of self-assembled InAs/GaAs NCs were evaluated.<sup>[97]</sup> The calculations included 21 NC systems with different shapes, sizes, and alloying profiles using atomistic empirical pseudopotential methods. The results agreed with the experimentally observed reductions of the exciton energy pressure coefficients when compared to bulk values. Furthermore, the calculations also demonstrated that the reductions are due to the nonlinear pressure coefficients  $\alpha$  of bulk GaAs and InAs.<sup>[97]</sup> Under hydrostatic pressure, the PL of  $\text{In}_{0.5}\text{Al}_{0.5}\text{As}$  NCs, another alloyed III–V material, was shown to blue-shift up to 0.8 GPa and exhibited an  $\alpha$  value of  $90 \text{ meV GPa}^{-1}$ .<sup>[98]</sup> Between 0.8 and 2.0 GPa, no significant shift in the PL was measured, and above 2.0 GPa, a gradual red-shifting was seen until the emission quenched at 2.6 GPa. It was argued that the three emission behaviors originated from three distinct pressure regions, thereby leading to three apparent band structures.<sup>[98]</sup> The experimentally determined  $\alpha$  value of  $90 \text{ meV GPa}^{-1}$  is smaller than that of bulk InAlAs but is consistent with that of InAs/GaAs NCs.<sup>[96]</sup> It was found that the relative decrease in  $\alpha$  (compared to the bulk) was due to the highly confined energy levels in the NCs, with similar phenomena reported for increasing confinement in InGaAs/AlGaAs quantum wells.<sup>[99]</sup>

The PL of InP/GaP NCs was studied as a function of temperature, laser illumination, and pressures up to 8 GPa (Figure 7).<sup>[100]</sup> At ambient pressure, the PL of InP/GaP NCs arises from direct optical transition between the lowest electron and hole in the gamma point states. It was suggested that at a pressure of approximately 0.15 GPa, a  $\Gamma_x$  conduction

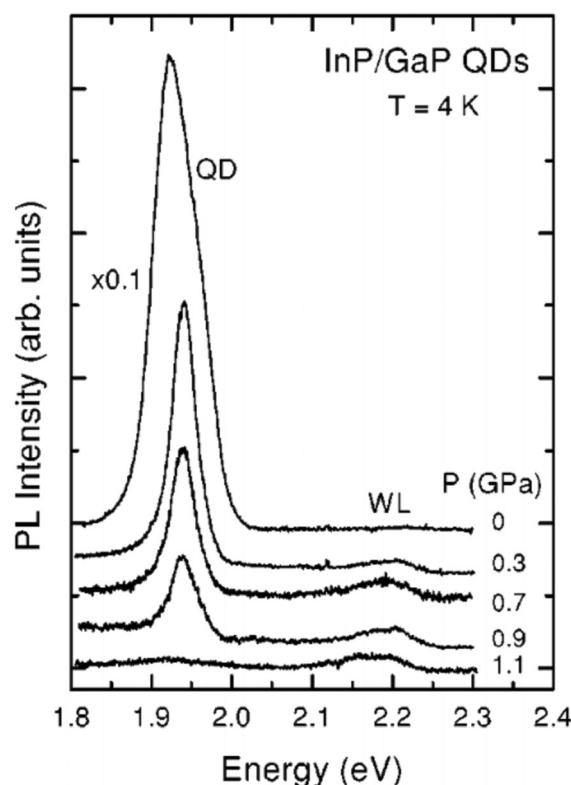


**Figure 7.** PL spectra of InP/GaP at 4 K at various pressures. The subtle blue-shift is noted. Reproduced from Ref. [100] with permission, copyright 2003 American Physical Society.

band crossover occurs, after which the emission intensity drops about 20-fold and exhibits a red-shift. These results imply that the InP/GaP has a type I band gap alignment up to 1.2 GPa. At pressures greater than 1.2 GPa, the emission was quenched, which signaled a transition to a type-II alignment.

Reduced dimensionality has been shown to increase the phase transition pressure (e.g. AlAs/GaAs superlattices,<sup>[101]</sup> Si NCs,<sup>[102]</sup> and the wurtzite to rock salt transition of CdSe NCs<sup>[80]</sup>), which has spurred investigation of other pressure-affected transitions. Reduced dimensionality was computationally found to cause a decrease in the pressure-induced transition from a direct to an indirect band gap in InP NCs.<sup>[103]</sup> It has been established that zincblende semiconductors experience a transition from a direct ( $\Gamma_{1c}$ ) to indirect ( $X_{1c}$ ) band gap when under pressure. Pressure has also been found to produce an increase in the energy of  $\Gamma_{1c}$  and a decrease in the energy of  $X_{1c}$ .<sup>[104,105]</sup> Calculations suggest that the quantum confinement from the reduced dimensionality of the InP NCs promotes a smaller separation of  $\Gamma_{1c}$  and  $X_{1c}$  compared to the bulk. As a consequence of their smaller initial separation, less pressure is needed to achieve overlap, which manifests as an electronic transition at a decreased pressure. In contrast to these computations, a subsequent experimental study has not found a reduction in the pressure-induced direct-to-indirect band gap transition of InP NCs, with both NCs and bulk InP experiencing a direct-to-indirect crossover at about 10 GPa.<sup>[106]</sup> It is suggested that the discrepancy between experiment and theory originates from over-simplifications

regarding bond lengths, potentials, and In/P ratios in the computations. Hydrostatic pressures up to 13 GPa were applied to two different-sized InP NCs.<sup>[106]</sup> For pressures up to 9 GPa, the PL spectra were found to display emitting states similar to that at ambient pressure, thus suggesting no electronic transition occurred. For both sizes of InP, a strong blue-shift (from  $\lambda \approx 640$  nm to  $\lambda \approx 520$  nm) was observed up to 9–10 GPa, at which point the PL is slightly red-shifted. Beyond 12.3 GPa, the band gap emission became extremely weak and was dominated by trap states.

### 2.2.3. IV–VI Semiconductors

PbSe is a popular IV–VI system for the synthesis of NCs. The optical properties of PbSe NCs were examined under pressures ranging from ambient to 5.4 GPa (Figure 8).<sup>[107]</sup> As a consequence of their relatively large Bohr radius of 46 nm, PbSe NCs are known to have an energy gap that is dominated by quantum confinement. Despite that fact, it was found that the energy gaps of all three tested sizes of PbSe NCs (3, 5, 7 nm) shifted monotonically with pressure, almost entirely determined by their bulk deformation potential. All three sizes of PbSe NCs were found to red-shift with increasing pressure, which is starkly different from the behavior of other NCs. This opposite phenomenon is in agreement with the fact that the bulk deformation potential of PbSe is negative, while that of CdSe is positive. The pressure coefficients  $\alpha$  for the 3, 5, and 7 nm NCs were found to be  $-47$ ,  $-54$ , and  $-56$  meV GPa $^{-1}$ , respectively. A clear inverse correlation between the absolute value of  $\alpha$  and nanocrystal size was found for PbSe NCs within the size range 3–13 nm, which is indicative of strong quantum confinement.<sup>[108]</sup> The  $\alpha$  values for the 13 and 3 nm PbSe NCs were revealed to be  $-76$  and  $-41$  meV GPa $^{-1}$ , respectively. Notably, the  $\alpha$  values for all tested PbSe NCs are smaller than that of bulk PbSe, which is  $-84$  meV GPa $^{-1}$ .<sup>[107,108]</sup>

PbS NCs, another IV–VI material, have also been explored for their pressure-dependent optical properties.<sup>[109]</sup>

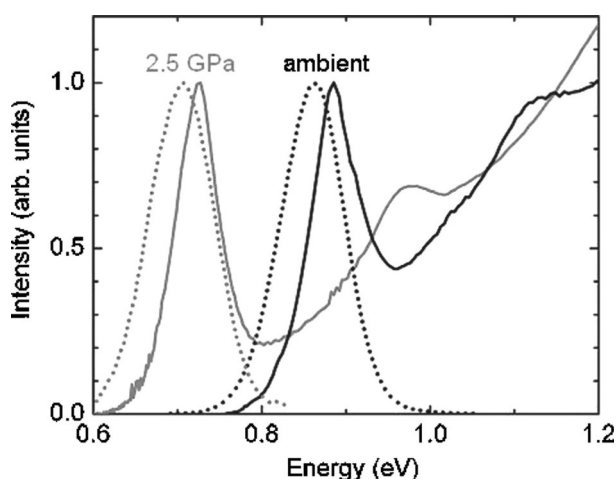


**Figure 8.** PL (dotted lines) and IR absorption (solid lines) of 5 nm PbSe NCs at ambient and 2.5 GPa pressures. Reproduced from Ref. [107] with permission, copyright 2007 American Institute of Physics Publishing.

Three different sizes of PbS NCs (small: 3 nm; intermediate: 3.7 nm; and large: 6.7 nm) were exposed to pressures ranging from 0 to 14.5 GPa, and the PL of all was found to consistently red-shift. Notably, the PL of larger PbS NCs was seen to red-shift more than smaller NCs, as evidenced by pressure coefficients of  $-40.6$ ,  $-50.1$ , and  $-61.0$  meV GPa $^{-1}$  for 3 nm, 3.7 nm, and 6.7 nm NCs, respectively. Theoretical calculations revealed that the size-dependence of the pressure coefficients originated from the size-dependent quantum confinement energy, the compressibility of the PbS cores, and, to a lesser degree, the exciton potential energy.

## 3. Anisotropic Pressure

This Minireview has so far centered only on NCs under uniform hydrostatic compression. In the next section, the focus will be on NCs under a variety of different anisotropic stress states. Anisotropic pressure is defined as pressure that stresses different axes in a non-uniform manner.

### 3.1. Anisotropic Static Compression of 0D Nanocrystals

The pressure-dependent PL of CdSe NCs was studied in several distinct pressure media, including an ethanol/methanol mixture, argon, NaCl, and silicon fluid, as well as in no medium at all.<sup>[110]</sup> As seen in Figure 9a, the application of pressure was observed to result in the PL energy either regularly increasing (in hydrostatic media: methanol/ethanol, Ar) or flattening/decreasing after an initial increase (in non-hydrostatic media: NaCl, silicon fluid; direct compression). The flattening/decrease of the PL was shown to arise from shearing effects produced from the non-hydrostatic pressure. The effects of uniaxial, biaxial, and triaxial pressure on the band gap of CdSe NCs were calculated using the semi-empirical pseudopotential method (Figure 9b). The calculations suggest that the application of hydrostatic pressure would lead to a continuous blue-shifting, whereas non-uniform pressure on other axes would induce vastly different results. The theoretical results seem to agree well with the divergent experimental PL behaviors.

The PL of individual CdSe/CdS/ZnS core/shell nanocrystals under anisotropic pressures up to 3.8 GPa was investigated by isolating individual NCs under an AFM cantilever.<sup>[111]</sup> To enable this study, a commercial AFM was mounted on top of a confocal fluorescence microscope, thereby allowing in situ characterization. It was seen that 33 % of trials resulted in red-shifts averaging  $-3.5$  meV GPa $^{-1}$  and 67 % of the trials resulted in blue-shifts averaging  $3.0$  meV GPa $^{-1}$ . These observations are in good agreement with previous calculations.<sup>[110]</sup> It was predicted that stress along different axes would result in different PL shifts. Assuming the NCs are randomly oriented, the ratio of blue-shifting to red-shifting could even be predicted.<sup>[110]</sup>

The PL evolution of two different sizes (2.3 and 5.1 nm) of CdTe NCs was studied under non-hydrostatic pressure conditions.<sup>[112]</sup> To achieve non-uniform pressure, CdTe powder was loaded in a DAC without a pressure medium. The

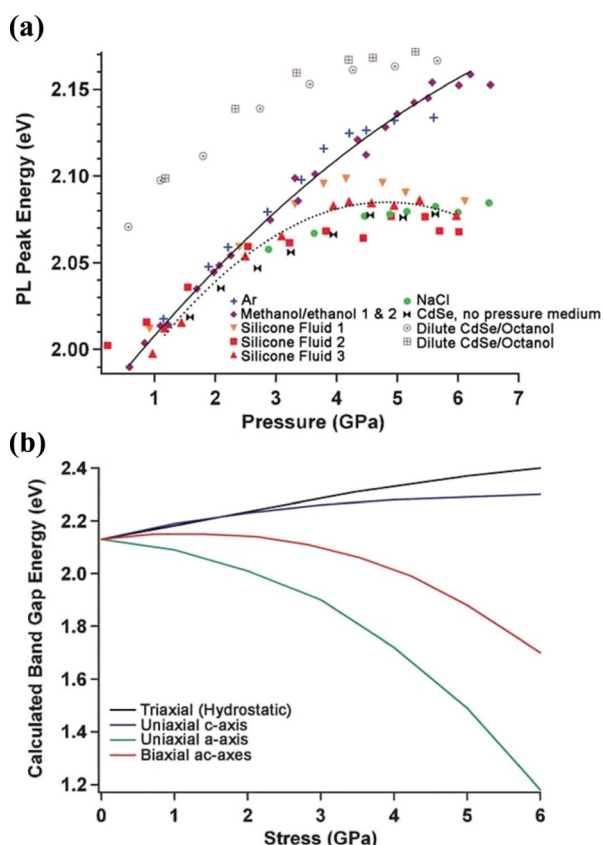


**Figure 9.** a) Pressure-dependent PL band energy evolution of CdSe QDs in several different pressure media including: liquid (4:1 methanol/ethanol), nonliquid (argon above 1.3 GPa, sodium chloride, and silicone fluid), and in the absence of any pressure medium. The solid and dotted lines illustrate the different PL band energy behaviors depending on uniform (solid line) or non-uniform (dotted line) stress environments.<sup>[110]</sup> b) Calculated band gap as a function of triaxial (hydrostatic) compression (black trace), uniaxial compression along the *a* and *c* axes (green and blue traces, respectively), and biaxial compression along the *a* and *c* axes (red trace). Hydrostatic compression yields a band gap that increases monotonically with increasing pressure. Uniaxial compression along the *c* axis shows a steady increase with pressure, but the magnitude is smaller than with hydrostatic compression. Uniaxial compression along the *a* axis or biaxial compression along the *a* and *c* axes results in a decrease in the band gap energy.<sup>[110]</sup> Reproduced from Ref. [110] with permission, copyright 2008 John Wiley and Sons.

emission wavelength was found to decrease and pass through a minimum of  $\lambda = 585$  nm at around 4.7 GPa and remain unchanged up to 6.1 GPa. Notably, the slope of the pressure-dependent band energy was noticed to decrease as the NC size increased, a similar trend as hydrostatically compressed CdTe NCs.<sup>[83]</sup> PL flattening is consistent with that seen from the shearing effects of non-hydrostatic pressure.<sup>[112]</sup> No flattening of the PL was observed in CdTe NCs under uniform hydrostatic pressure.<sup>[83]</sup>

The optical properties of GaAs NCs were also examined under uniaxial tensile stress.<sup>[113]</sup> A semiconductor membrane with epitaxially grown GaAs NCs was placed on a piezoelectric actuator capable of inducing 0.2 % strain. As a result of the geometry of this device, uniaxial pressures of about

1.3 GPa were achieved. The application of uniaxial stress was found to result in an increased emission intensity and the red-shifting of the PL band from  $\lambda \approx 770$  to 830 nm, a total energy shift of over 100 meV. Most notably, the application of uniaxial pressure facilitated a flip in the quantization of the axis of the GaAs NCs into the growth plane, which is of great interest for integrated quantum photonic applications.

### 3.2. Anisotropic Static Compression of Complex Geometry Nanocrystals

Nanocrystals can have geometries more complex than the zero-dimensional QDs previously described. The pressure-dependence of the optical properties of CdSe/CdS core/shell QDs, nanorods, and CdSe/CdS core/arm tetrapods were studied.<sup>[114]</sup> The tested nano-tetrapods (denoted tQDs) consist of a CdSe core with four CdS arms branched at a tetrahedral angle. It has been previously demonstrated that tQD arms flex with the application of only 100 nN of force.<sup>[115]</sup> It has since been theoretically calculated that arm bending results in a reduction of symmetry, which influences the energy levels and causes a red-shift of the emission.<sup>[116]</sup> Different tQD samples were dispersed in a hydrostatic (pentane/isopentane) and non-hydrostatic (toluene) pressure media and then loaded into a diamond anvil cell. As toluene freezes at 1.7 GPa and shows high viscosity above ambient pressure, it functions as a highly anisotropic, non-hydrostatic pressure transmitting medium. Under hydrostatic pressure, all the particle geometries (QDs, nanorods, tQDs) showed a monotonic blue-shift and a slight asymmetric broadening of their band emission at longer wavelengths as the pressure increased. In the non-hydrostatic testing, unique geometries responded differently. The PL of QDs split into a doublet above 0.7 GPa, QDs and nanorods have an additional shallow PL band at  $\lambda \approx 650$  nm, and, in contrast to the other two geometries, tQDs displayed red-shifted PL as the pressure increased. The complete PL spectra of each geometry under different pressures are shown in Figure 10. All the PL changes were found to be reversible after removal of pressure, with no measured hysteresis. The lack of an abrupt decrease in the PL intensity suggests that there was no phase transition to rock salt, which was attributed to the mechanically stiffer CdS on the surface of all the particle geometries.<sup>[117]</sup> The fluorescent response of tQDs to non-hydrostatic stress in a simple uniaxial geometry was calibrated with the aim of using CdSe/CdS tQDs as luminescent nanocrystal stress gauges.<sup>[118]</sup> Nanosized tQDs were incorporated into single polyester fibers, and their PL was monitored under tensile strain. A clear red-shift was observed as the strain increased, with a band gap pressure coefficient of  $-5.8$  meV GPa<sup>-1</sup>. The use of tQDs as in situ stress gauges in fibers is of particular interest because identifying the real-time true stress of fibers is nearly impossible because of their pressure-induced change in dimensionality. A similar study involved electrospinning up to 40 wt % CdSe/CdS tQDs into poly(L-lactic acid).<sup>[119]</sup> The PL of the tQDs red-shifted by about 10 meV as the electrospun fibers reached 0.3 strain. The PL of CdSe/CdS tQDs dispersed in a poly(styrene-ethylene-butylene-styrene)



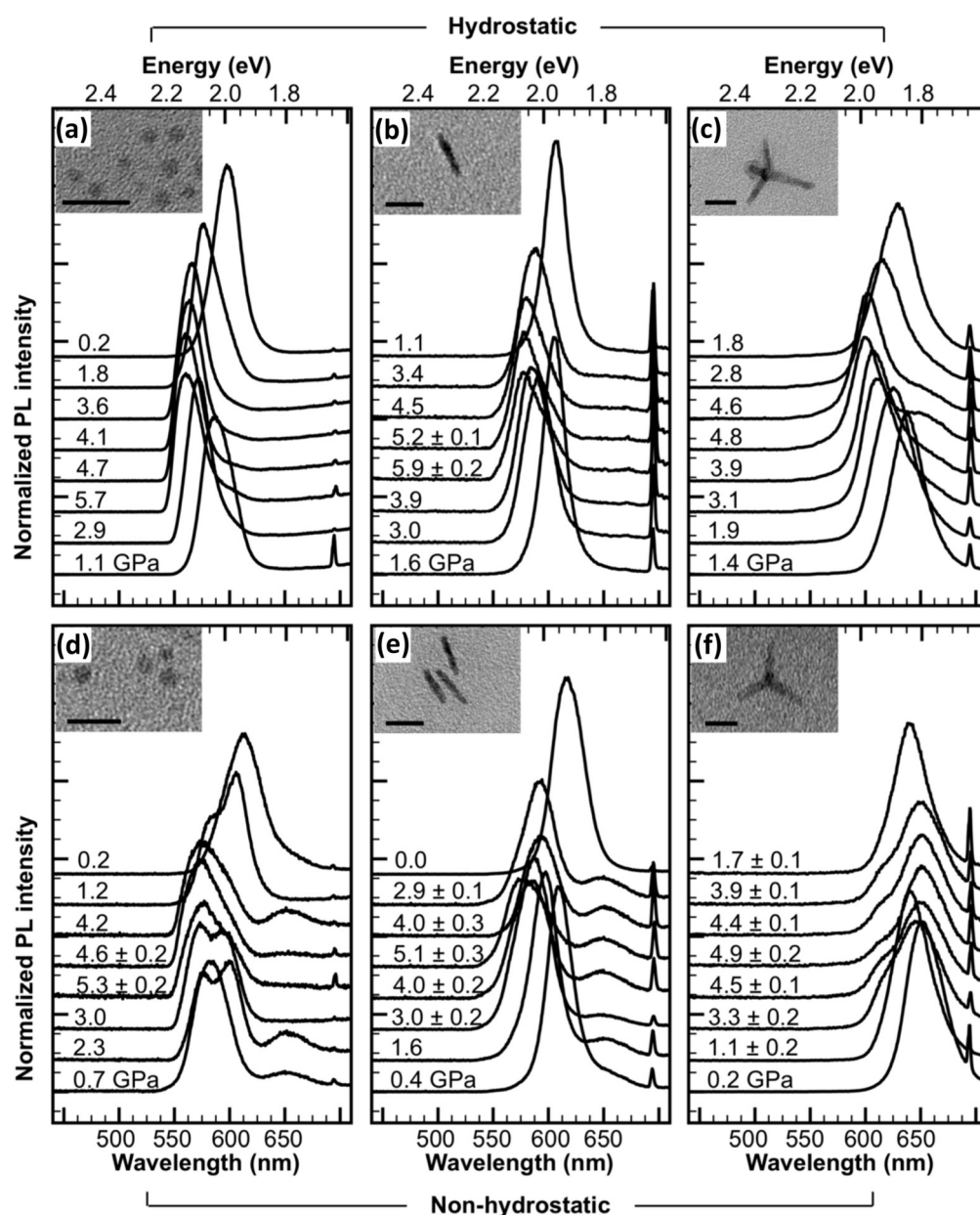


**Figure 10.** PL evolution from NCs of various geometries under different pressure states. a,d) 0D quantum dots; b,e) 2D nanorods, c,f) 3D tQDs; a–c) were evaluated under hydrostatic pressure, and d–f) under non-hydrostatic pressure. Reproduced from Ref. [114] with permission, copyright 2009 American Chemical Society.

(SEBS) matrix was tracked under applied tensile stress.<sup>[120]</sup> Solvent was evaporated quickly under  $N_2$  flow for some samples and others were allowed to evaporate slowly under ambient conditions. After application of tensile stress, the quickly dried composites exhibited a red-shift and the slowly dried samples a blue-shift. This divergent behavior was found to be due to solvent drying affecting the grouping of the tQDs.<sup>[120]</sup> Slowly drying the composites enabled the formation of small, dense assemblies of tQDs, which were compression-sensing. The quick drying preferentially led to the formation of larger tQD aggregates, which were shown to result in tension within the tQDs. DFT calculations were performed to confirm these hypotheses.

The pressure dependence of the PL of 2D CdSe nanoplatelets (NPs) was also investigated.<sup>[121]</sup> Four and five monolayer (ML) CdSe NPs were loaded into a DAC with silicone liquid as the pressure medium. It was found that as the pressure increased, the PL of the NPs blue-shifted monotonically (ca. 11 and 7 nm, for 4 and 5 ML, respectively) until the pressure reached about 2 GPa. After this pressure, the PL of both NPs shifted towards longer wavelengths and displayed a broadening of the PL spectra until quenching at 7.7 (4ML) and 7.2 GPa (5ML), respectively. This PL behavior is starkly different from the monotonic blue-shift previously observed for CdSe QDs<sup>[73]</sup> and is summarized in Figure 11. The initial blue-shift of the PL of both NPs was attributed to lattice contraction, which narrowed the quantum wells. Several explanations were given for the red-shift, including 1) a pressure-induced intermediate phase, 2) pressure-induced ligand reconstruction, and 3) bands originating from the pressure media and compression environment, among which a pressure-induced ligand effect was determined to likely be the dominant mechanism.

### 3.3. Anisotropic Dynamic Compression of Nanocrystals

Shock testing is a dynamic non-uniform pressure that has been used to scrutinize the PL characteristics of NCs. Shock experiments were made more accessible by the Dlott group at UIUC by utilizing laser-launched flyer plates instead of gas guns.<sup>[122,123]</sup> In the simplest terms, a laser strikes a metal foil, thereby instantly transforming it into plasma, which creates a shockwave that propagates through the sample material. As the focus of this Minireview is on the optical properties of NCs, no further description of shock pressure will be

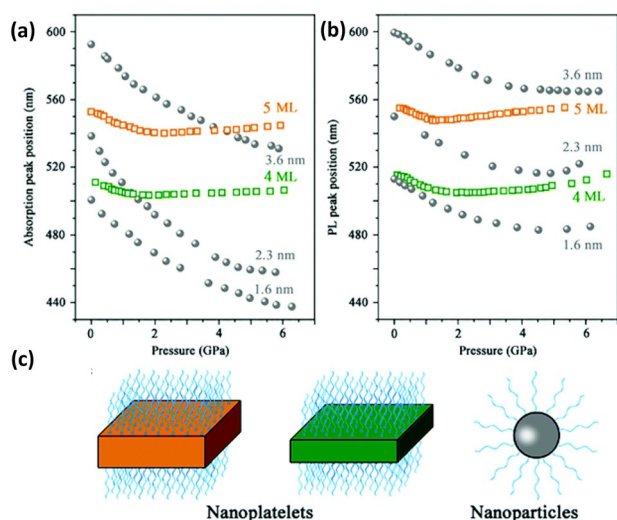


**Figure 11.** Morphology- and size-dependent optical behaviors of CdSe NCs under high pressure. a) Pressure-dependent absorption spectra; b) pressure-dependent PL spectra; and c) schematic representation of the CdSe NPLs and QDs. Reproduced from Ref. [121] with permission, copyright 2015 Royal Society of Chemistry.

discussed, interested readers are encouraged to see the relevant literature.<sup>[122–126]</sup> The effect of shock pressure on the PL emission of CdTe NCs was inspected.<sup>[127]</sup> In the study, poly(vinyl alcohol) (PVA) matrixes were loaded with 0.15 wt% CdTe NCs and subjected to pressures up to 7.3 GPa. Upon impact of the shockwave, the emission of the NCs was found to blue-shift by a maximum of 5.2 nm at 4.3 GPa, and return to a wavelength only 1.6 nm blue-shifted from the original. This behavior is significantly different from the monotonic increasing blue-shift displayed by CdTe NCs under hydrostatic pressure.<sup>[79,83,84]</sup> Such differences can be attributed largely to the different stress states achieved in the shock and hydrostatic experiments and the time-dependence of the mechanical response of the polymer matrix. In a follow-up study, CdTe NCs were explored as mesoscale pressure sensors; the results from the shock test are shown in Figure 12.<sup>[128]</sup> NCs possess many attractive features for application as in situ diagnostic tools including their nanometer size, tunable narrow photoluminescent emission, broad absorption, fast photoluminescent decay, and negligible light scattering. CdTe NCs in both soft PVA and hard inorganic sodium silicate glass matrixes were tested with shock pressures ranging from 2.0 to 13.0 GPa (higher pressures than in Ref. [127]). NCs in both hard and soft matrixes featured a shock-induced blue-shift and intensity loss. Time-resolved PL measurements allowed the observation of PL evolution as the shock wave propagated through the sample. Understanding the time-resolved PL shift is critically important for using these NCs as in situ pressure sensors. The blue-shift of the emission of NCs in both the polymer and glass displayed the same non-monotonic increase as seen in a previous study.<sup>[127]</sup> The turnover pressure (pressure at which the blue-shift reaches a maximum and starts decreasing) was about 4 GPa in polymer and 9 GPa in the glass matrix. When CdSe NCs were studied under shock compression at up to 3.75 GPa,

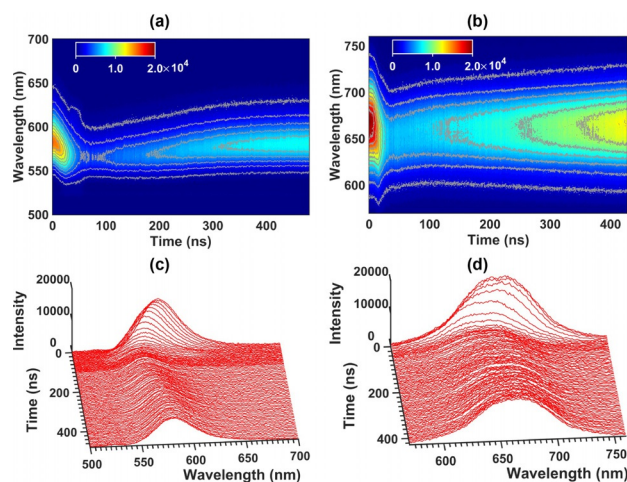


**Figure 12.** Time-resolved PL measurements during shock compression of CdTe in a,c) poly(vinyl alcohol) and b,d) glass matrixes. Reproduced from Ref. [128] with permission, copyright 2016 American Institute of Physics Publishing.

a near complete disappearance of the first excitonic feature and broadening of the low energy absorption edge was observed at 3 GPa, which indicates a wurtzite to rock salt structural transition.<sup>[130]</sup> This phase transition pressure is much lower than that previously reported for hydrostatic pressure (7.5 GPa).<sup>[80]</sup> The decrease in the transition pressure is ascribed to shock-induced shear stress along the reaction coordinate.<sup>[130]</sup>

#### 4. Summary and Outlook

In summary, the application of uniform and non-uniform pressure has been shown to greatly affect the optical properties of a variety of semiconductor NCs. Hydrostatic pressure (i.e. uniform pressure) was demonstrated to alter the optical properties of different perovskite nanocrystals in vastly different ways.<sup>[49–59]</sup> Pressure-induced perturbations of the lead–halide bond length and bond angles were identified to be the leading cause of the shifted optical properties. Hydrostatic pressure was found to trigger a blue-shift in the PL of all NCs made of type II–VI and type III–V semiconductors, thereby resulting in positive band gap pressure coefficients.<sup>[65–100]</sup> The increase in the band gap was attributed to enhanced orbital overlap as a result of pressure-induced lattice contraction. Interestingly, type IV–VI semiconductor NCs were observed to possess an opposite trend, with uniform pressure leading to consistent red-shifts.<sup>[107–109]</sup> The opposite trend was determined to be due to the enhanced effects of quantum confinement as a result of the large Bohr radius of lead.

The effect of non-uniform pressure (i.e. anisotropic static and dynamic pressures) on the optical properties of semiconductor NCs was also reviewed. Shearing from anisotropic static pressure was shown to flatten and even change the sign of the pressure-induced PL shifts of 0D QDs.<sup>[110–112]</sup> The PL behavior of complex geometry CdSe/CdS NCs, nanorods, and tetrapods under both uniform and non-uniform pressure was

surveyed, and the PL response of each geometry to different pressure states can be seen in Figure 10.<sup>[114–121]</sup> The PL of 0D NCs subjected to highly anisotropic shock pressures were shown to initially blue-shift and eventually red-shift to their original position.<sup>[127–129]</sup> The unique behavior observed in these studies was ascribed to the complex interactions that dynamic shockwaves have on the loading matrixes.

Although this Minireview highlights much of the progress made in understanding the pressure-dependence of PL in semiconductor NCs, the field is ripe for additional investigation. Achieving a more definitive value for the pressure coefficient  $\alpha$  is one area for future investigation. The conflicting reports on the  $\alpha$  value of CdSe<sup>[73–77]</sup> suggest the difficulty in obtaining accurate values. The need for precise  $\alpha$  values is essential for a variety of reasons. As discussed below, the application of CdSe NCs as optomechanical sensors is contingent upon the rigorous calibration of applied pressure and emission shift. Additionally, comparing the  $\alpha$  value of bulk and NC semiconductors represents a powerful method to better isolate the effect of quantum confinement from pressure and optical properties, and cannot be properly analyzed without precise  $\alpha$  values.

Further exploration of the pressure-dependence of the PL of various perovskite materials is also a promising future direction. Although all-inorganic CsPbX<sub>3</sub><sup>[46,51,55,56,61]</sup> and organolead APbX<sub>3</sub><sup>[65,67]</sup> perovskite NCs have been studied, a diversity of other compositions remain unexamined. Perovskites containing mixed cations such as (Cs<sub>a</sub>MA<sub>b</sub>FA<sub>1–a–b</sub>)PbX<sub>3</sub><sup>[130]</sup> and (Cs<sub>a</sub>MA<sub>b</sub>FA<sub>c</sub>Rb<sub>1–a–b–c</sub>)PbX<sub>3</sub><sup>[131]</sup> have been shown to possess enhanced optical properties and superior stability. The markedly improved stability has been attributed to the altered strain state of the lattice from the inclusion of additional ions.<sup>[132]</sup> The PL quenching of perovskite NCs has been documented at pressures as low as 1.3 GPa, far below that endured by conventional semiconductors.<sup>[51]</sup> In this context, the incorporation of additional ions may maintain the perovskite stability and increase the maximum pressure prior to quenching.

The pressure-dependence of the PL of complex perovskite NCs represent another research direction with great potential. It has been shown that CdSe/CdS NCs with different geometries (e.g. 0D QDs, 1D nanorods, 3D tetrapods) carry distinct pressure-dependent PL characteristics.<sup>[114]</sup> Perovskite NCs can also be synthesized to possess unique geometries, but their pressure-dependent PL remains unknown. 2D metal halide perovskite nanoplatelets can be formed by using A-site cations too large to fit within the 3D perovskite lattice.<sup>[133,134]</sup> Hollow nanocages,<sup>[135]</sup> 1D nanorods,<sup>[136]</sup> and 1D nanowires<sup>[137]</sup> of metal halide perovskite materials have also been readily crafted. Each of these geometries could have singular pressure-dependent optical properties and is worth scrutinizing.

Understanding the effects of non-ideal NC dispersion on pressure-induced PL behavior is also a direction that merits future research. Most studies were conducted with well-dispersed samples, effectively enabling each NC to be ideally and universally compressed. When sample loading is increased, NCs can aggregate or exist in proximity, which could lead to a variety of interesting factors, including self-

absorption and interactions between the NCs. Altering the loading on the sample changes the relevant phenomenon from a simple one-body event to a much more complex multibody problem. These more intricate interactions could exert a profound influence on the pressure-dependent PL and thus invites future work.

Obtaining a more robust modeling strategy for semiconductor NCs under various non-uniform pressures is also of great future interest. Most theoretical calculations have been based on the hydrostatic uniform compression of NCs, but many practical pressure conditions are anisotropic and dynamic. These non-uniform pressures could either compress or elongate different coordinates of the NC, which could have different effects on the PL. NCs are not necessarily isotropic, with strains in different crystallographic directions, thereby resulting in disparate PL behavior. Developing more vigorous computational models of NCs under high pressure may illuminate this currently unknown field.

The knowledge gained from research into the pressure-dependence of the PL of semiconductor NCs could lead to next-generation in situ optomechanical sensors. With an explicit understanding of the PL changes expected from an array of NCs, observed PL changes could be calibrated and correlated to sense unknown pressures experienced by a material. NCs could be embedded into a matrix and allow the real-time mapping of pressure evolution from the shifts in the PL from the affected NCs. A variety of compositions and geometries of NCs could be employed to ensure that the encapsulated NCs emit over a variety of pressures and to broaden the range of signals, thus rendering easier detection. Although the NCs discussed in this Minireview emit within the visible range, NCs emitting in the UV,<sup>[138]</sup> NIR,<sup>[139]</sup> or IR<sup>[140]</sup> ranges could also be utilized to further expand the detectable signals. Capitalizing on NCs with different emissive wavelengths could allow mesoscale sensing, with the multiplexed response yielding new spatial information. NCs loaded into a variety of matrixes could lead to a better understanding of the pressure evolution in a variety of novel matrix materials.

One particularly promising application for NCs as in situ pressure sensors is in 2D shock pressure mapping of heterogeneous energetic materials and mesoscale dynamic pressure diagnostics. The behavior of heterogeneous materials under shock compression is highly dependent on mesoscale effects from the collapse of voids and interactions between the shock wave and material inhomogeneities.<sup>[127,128]</sup> Understanding the influence of these mesoscale inhomogeneities on the evolution of pressure in the bulk material is of critical importance, but is difficult with current technologies. By embedding semiconductor NCs in these materials and monitoring their PL shifts, real-time spatially resolved pressure maps could be extracted. These pressure maps could provide information on the stress states around heterogeneities and assist in the understanding and design of future samples. Inorganic semiconductor NCs are especially attractive for this application because their nanosize allows for seamless integration into nearly any system and their hardy mechanical properties enable them to survive the elevated temperatures and



pressures (reaching the GPa range) that are common with dynamic shock testing.

Another exciting device-scale application for the pressure-altered optical properties of NCs is in quantum photonic circuits. Quantum photonic circuits are devices that utilize photons as carriers of information. Photons represent an attractive option for quantum data transfer because they are low noise carriers that do not suffer from the same decoherence as matter-based quantum systems.<sup>[141]</sup> Integrated photonic circuits have wide-reaching applications in computing and communication but necessitate the development of materials that reliably produce information-containing photons.

Semiconductor NCs are a promising material for the emission of single and entangled photons for emerging quantum technologies.<sup>[142,143]</sup> The natural quantization axis of NCs is generally parallel to their growth direction, which is beneficial for vertically emitting devices, but detrimental for planar photonic circuits. Uniaxial pressure from a device-scale piezoelectric actuator has been shown to ideally orient transition dipoles and oscillator strengths for integrated quantum photonics.<sup>[113]</sup> The rational design of devices with NCs under uniaxial tension may also lead to the emission of polarization-entangled photon pairs or single-photon sources with enhanced recombination rates and indistinguishability levels. This study represents an exciting new direction, where the application of easily achievable pressures could enable the use of various semiconductor NCs as emitters in next-generation integrated photonic circuits. This result has already spurred the further study of NCs for this application.<sup>[143–145]</sup>

Further study of other NC compositions could broaden the library of materials for photonic applications. It is urgent to determine if the quantization axis of other NCs can be tuned by the application of uniaxial pressure. In particular, perovskite NCs could be excellent candidates because of their characteristic high PLQYs and defect tolerance. In addition to perovskite NCs, all the other compositions summarized in this Minireview should also be explored for their use in pressure-enhanced quantum photonic applications. By utilizing the pressure-dependent optical properties of NCs, a strong repository of effective emitters could be built to meet the demands of future quantum technologies.

The pressure-dependent PL behavior of semiconductor NCs offers a glimpse into the interactions of physical manipulation, electronic distortion, and quantum confinement. Although the behavior of traditional semiconductor nanomaterials under hydrostatic pressure has been the most extensively studied, there is still room for refinement and enhanced precision. Additionally, relatively new additions to the field including metal halide perovskites, complex geometries, and novel pressure states open new avenues for continued exploration.

## Acknowledgements

This work is supported by the DOD-DTRA (HDTRA1-18-1-0004), the NSF (CMMI 1914713, DMR 1903990, and ECCS 1914562).

## Conflict of interest

The authors declare no conflict of interest.

- [1] F. Bai et al., *MRS Bull.* **2015**, *40*, 961–969.
- [2] B. Li et al., *Nat. Commun.* **2017**, *8*, 1–9.
- [3] B. Li, X. Wen, R. Li, Z. Wang, P. G. Clem, H. Fan, *Nat. Commun.* **2014**, *5*, 1–7.
- [4] F. Bai et al., *Adv. Mater.* **2016**, *28*, 1989–1993.
- [5] A. P. Alivisatos, *Science* **1996**, *271*, 933–937.
- [6] B. P. Aryal, D. E. Benson, *J. Am. Chem. Soc.* **2006**, *128*, 15986–15987.
- [7] Y. Zhao, C. Riemersma, F. Pietra, R. Koole, C. De Mello Donegá, A. Meijerink, *ACS Nano* **2012**, *6*, 9058–9067.
- [8] W. W. Yu, E. Chang, R. Drezek, V. L. Colvin, *Biochem. Biophys. Res. Commun.* **2006**, *348*, 781–786.
- [9] A. Jaffe, Y. Lin, W. L. Mao, H. I. Karunadasa, *J. Am. Chem. Soc.* **2015**, *137*, 1673–1678.
- [10] W. L. Mao et al., *Proc. Natl. Acad. Sci. USA* **2010**, *107*, 9965–9968.
- [11] Y. Ma et al., *Nature* **2009**, *458*, 182–185.
- [12] G. Xiao, C. Zhu, Y. Ma, B. Liu, G. Zou, B. Zou, *Angew. Chem. Int. Ed.* **2014**, *53*, 729–733; *Angew. Chem.* **2014**, *126*, 748–752.
- [13] A. L. Edwards, H. G. Drickamer, *Phys. Rev.* **1961**, *122*, 1149–1157.
- [14] J. Li, L. W. Wang, *Appl. Phys. Lett.* **2004**, *85*, 2929–2931.
- [15] K. Jacobs, A. P. Alivisatos, *Rev. Mineral. Geochemistry* **2001**, *44*, 59–72.
- [16] S. H. Tolbert, A. P. Alivisatos, *Annu. Rev. Phys. Chem.* **1995**, *46*, 595–626.
- [17] F. Bai, K. Bian, X. Huang, Z. Wang, H. Fan, *Chem. Rev.* **2019**, *119*, 7673–7717.
- [18] Q. A. Akkerman et al., *Nat. Energy* **2017**, *2*, 16194.
- [19] F. Zhou, Z. Li, H. Chen, Q. Wang, L. Ding, Z. Jin, *Nano Energy* **2020**, *73*, 104757.
- [20] M. Hao et al., *Nat. Energy* **2020**, *5*, 79–88.
- [21] A. Swarnkar et al., *Science* **2016**, *354*, 92–95.
- [22] Y. Chang et al., *ACS Appl. Mater. Interfaces* **2018**, *10*, 37267–37276.
- [23] Y. He et al., *Sci. Adv.* **2019**, *5*, eaax4424.
- [24] Y. J. Yoon et al., *Adv. Mater.* **2019**, 1901602.
- [25] M. Yuan et al., *Nat. Nanotechnol.* **2016**, *11*, 872–877.
- [26] X. Du et al. *RSC Adv.* **2017**, 10391–10396.
- [27] D. H. Kwak, D. H. Lim, H. S. Ra, P. Ramasamy, J. S. Lee, *RSC Adv.* **2016**, *6*, 65252–65256.
- [28] P. Ramasamy, D. H. Lim, B. Kim, S. H. Lee, M. S. Lee, J. S. Lee, *Chem. Commun.* **2016**, *52*, 2067–2070.
- [29] Q. Chen et al., *Nature* **2018**, *561*, 7721.
- [30] M. A. Green, A. Ho-Baillie, H. J. Snaith, *Nat. Photonics* **2014**, *8*, 506–514.
- [31] W.-J. Yin, T. Shi, Y. Yan, *Adv. Mater.* **2014**, *26*, 4653–4658.
- [32] A. Miyata et al., *Nat. Phys.* **2015**, *11*, 582–587.
- [33] D. Shi et al., *Science* **2015**, *347*, 519–522.
- [34] W. Zhang, G. E. Eperon, H. J. Snaith, *Nat. Energy* **2016**, *1*, 16048.
- [35] W. Nie et al., *Science* **2015**, *347*, 522–525.
- [36] H. Huang, M. I. Bodnarchuk, S. V. Kershaw, M. V. Kovalenko, A. L. Rogach, *ACS Energy Lett.* **2017**, *2*, 2071–2083.

- [37] D. N. Dirin et al., *Nano Lett.* **2016**, *16*, 5866–5874.
- [38] M. Pandey, K. W. Jacobsen, K. S. Thygesen, *J. Phys. Chem. Lett.* **2016**, *7*, 4346–4352.
- [39] D. Liu, T. L. Kelly, *Nat. Photonics* **2014**, *8*, 133–138.
- [40] Q. Fan, G. V. Biesold-McGee, J. Ma, Q. Xu, S. Pan, J. Peng, Z. Lin, *Angew. Chem. Int. Ed.* **2020**, *59*, 1030–1046; *Angew. Chem.* **2020**, *132*, 1042–1059.
- [41] L. Wu, et al., *Nano Lett.* **2017**, *17*, 5799–5804.
- [42] Y. Tong et al., *Angew. Chem. Int. Ed.* **2016**, *55*, 13887–13892; *Angew. Chem.* **2016**, *128*, 14091–14096.
- [43] Y. Hassan et al., *J. Am. Chem. Soc.* **2019**, *141*, 1269–1279.
- [44] F. Zhang et al., *ACS Nano* **2015**, *9*, 4533–4542.
- [45] L. Protesescu et al., *Nano Lett.* **2015**, *15*, 3692–3696.
- [46] Q. A. Akkerman, et al., *J. Am. Chem. Soc.* **2015**, *137*, 10276–10281.
- [47] M. C. Brennan, J. Zinna, M. Kuno, *ACS Energy Lett.* **2017**, *2*, 1487–1488.
- [48] V. M. Goldschmidt, *Naturwissenschaften* **1926**, *14*, 477–485.
- [49] A. Swarnkar, R. Chulliyil, V. K. Ravi, M. Irfanullah, A. Chowdhury, A. Nag, *Angew. Chem. Int. Ed.* **2015**, *54*, 15424–15428; *Angew. Chem.* **2015**, *127*, 15644–15648.
- [50] G. H. Ahmed, J. Yin, O. M. Bakr, O. F. Mohammed, *J. Chem. Phys.* **2020**, *152*, 020902.
- [51] G. Xiao et al., *J. Am. Chem. Soc.* **2017**, *139*, 10087–10094.
- [52] L. Zhang, Q. Zeng, K. Wang, *J. Phys. Chem. Lett.* **2017**, *8*, 3752–3758.
- [53] J. C. Beimborn, L. R. Walther, K. D. Wilson, J. M. Weber, *J. Phys. Chem. Lett.* **2020**, *11*, 1975–1980.
- [54] S. Yesudhas et al., *Chem. Mater.* **2020**, *32*, 785–794.
- [55] Y. Nagaoka, K. Hills-Kimball, R. Tan, R. Li, Z. Wang, O. Chen, *Adv. Mater.* **2017**, *29*, 1606666.
- [56] Y. Cao et al., *J. Phys. Chem. C* **2018**, *122*, 9332–9338.
- [57] G. Yuan, S. Qin, X. Wu, H. Ding, A. Lu, *Phase Transitions* **2018**, *91*, 38–47.
- [58] J. C. Beimborn, L. M. G. Hall, P. Tongying, G. Dukovic, J. M. Weber, *J. Phys. Chem. C* **2018**, *122*, 11024–11030.
- [59] J. Zhang et al., *Nanoscale* **2019**, *11*, 11660–11670.
- [60] Y. Cao et al., *ACS Mater. Lett.* **2020**, *2*, 381–388.
- [61] Z. Ma et al., *Nat. Commun.* **2018**, *9*, 4–11.
- [62] K. M. McCall, C. C. Stoumpos, S. S. Kostina, M. G. Kanatzidis, B. W. Wessels, *Chem. Mater.* **2017**, *29*, 4129–4145.
- [63] R. Fu et al., *Nanoscale* **2019**, *11*, 17004–17009.
- [64] T. Yin et al., *Adv. Mater.* **2018**, *30*, 1705017.
- [65] Y. Wang et al., *J. Am. Chem. Soc.* **2015**, *137*, 11144–11149.
- [66] T. Yin et al., *J. Am. Chem. Soc.* **2019**, *141*, 1235–1241.
- [67] H. Zhu et al., *J. Phys. Chem. Lett.* **2018**, *9*, 4199–4205.
- [68] L. Wang, K. Wang, B. Zou, *J. Phys. Chem. Lett.* **2016**, *7*, 2556–2562.
- [69] G. Liu et al., *Adv. Funct. Mater.* **2017**, *27*, 1604208.
- [70] M. Nirmal, D. J. Norris, M. Kuno, M. G. Bawendi, A. L. Efros, M. Rosen, *Phys. Rev. Lett.* **1995**, *75*, 3728–3731.
- [71] A. P. Alivisatos, *Science* **1996**, *271*, 933–937.
- [72] X. Peng et al., *Nature* **2000**, *404*, 59–61.
- [73] J. Li, G. H. Li, J. B. Xia, J. B. Zhang, Y. Lin, X. R. Xiao, *J. Phys. Condens. Matter* **2001**, *13*, 2033–2043.
- [74] B. S. Kim, M. A. Islam, L. E. Brus, I. P. Herman, *J. Appl. Phys.* **2001**, *89*, 8127.
- [75] J. N. Wickham, A. B. Herhold, A. P. Alivisatos, *Phys. Rev. Lett.* **2000**, *84*, 923–926.
- [76] A. P. Alivisatos, T. D. Harris, L. E. Brus, A. Jayaraman, *J. Chem. Phys.* **1988**, *37*, 8958–8981.
- [77] R. W. Meulenberg, G. F. Strouse, *Phys. Rev. B* **2002**, *66*, 353171–353176.
- [78] W. Shan, W. Walukiewicz, J. W. Ager, K. M. Yu, J. Wu, E. E. Haller, *Appl. Phys. Lett.* **2004**, *84*, 67.
- [79] J. R. Mei, V. Lemos, *Solid State Commun.* **1984**, *52*, 785–788.
- [80] S. H. Tolbert, A. P. Alivisatos, *J. Chem. Phys.* **1995**, *102*, 4642–4656.
- [81] S. H. Tolbert, A. P. Alivisatos, *Science* **1994**, *265*, 373–376.
- [82] S. H. Tolbert, A. B. Herhold, C. S. Johnson, A. P. Alivisatos, *Phys. Rev. Lett.* **1994**, *73*, 3266–3269.
- [83] Y.-C. Lin, *Proc. SPIE*, **2015**, 9373, 93730L.
- [84] F. X. Wu, J. M. Zaug, C. E. Young, J. Z. Zhang, *J. Nanosci. Nanotechnol.* **2008**, *8*, 6528–6532.
- [85] N. R. C. Corsini, N. D. M. Hine, P. D. Haynes, C. Molteni, *Nano Lett.* **2017**, *17*, 1042–1048.
- [86] Z. Zhao, J. Zeng, Z. Ding, X. Wang, J. Hou, Z. Zhang, *J. Appl. Phys.* **2007**, *102*, 1–4.
- [87] S. H. Wei, A. Zunger, *Phys. Rev. B* **1988**, *37*, 8958–8981.
- [88] S. H. Wei, A. Zunger, *Phys. Rev. B* **1988**, *37*, 8958–8981.
- [89] P. Lv et al., *J. Phys. Chem. Lett.* **2020**, *11*, 920–926.
- [90] J. Li, L. W. Wang, *Appl. Phys. Lett.* **2004**, *84*, 3648–3650.
- [91] V. S. Shusta, A. G. Slivka, O. O. Gomonnai, Y. M. Azhniuk, V. V. Lopushansky, *J. Phys. Conf. Ser.* **2008**, *121*, 162001.
- [92] J. Huso et al., *Appl. Phys. Lett.* **2006**, *89*, 171909.
- [93] K. B. Ford, et al., *Mater. Lett.* **2013**, *106*, 301–303.
- [94] B. Li et al., *Phys. Lett. Sect. A* **2019**, *383*, 1483–1486.
- [95] I. E. Itskevich, et al., *Appl. Phys. Lett.* **1997**, *70*, 505.
- [96] B. S. Ma et al., *J. Appl. Phys.* **2004**, *95*, 933–938.
- [97] J.-W. Luo, S.-S. Li, J.-B. Xia, L.-W. Wang, *Phys. Rev. B* **2005**, *71*, 245315.
- [98] J. Phillips, P. Bhattacharya, U. Venkateswaran, *Appl. Phys. Lett.* **1999**, *74*, 1549–1551.
- [99] V. A. Wilkinson, A. D. Prins, D. J. Dunstan, L. K. Howard, M. T. Emeny, *J. Electron. Mater.* **1991**, *20*, 509–516.
- [100] A. R. Goñi, C. Kristukat, F. Hatami, S. Dreßler, W. T. Masselink, C. Thomsen, *Phys. Rev. B* **2003**, *67*, 075306.
- [101] B. A. Weinstein, S. K. Hark, R. D. Burnham, R. M. Martin, *Phys. Rev. Lett.* **1987**, *58*, 781–784.
- [102] S. H. Tolbert, A. B. Herhold, L. E. Brus, A. P. Alivisatos, *Phys. Rev. Lett.* **1996**, *76*, 4384–4387.
- [103] H. Fu, A. Zunger, *Phys. Rev. Lett.* **1998**, *80*, 5397–5400.
- [104] D. J. Wolford, J. A. Bradley, *Solid State Commun.* **1985**, *53*, 1069–1076.
- [105] S. Ernst, A. R. Goñi, K. Syassen, M. Cardona, *Phys. Rev. B* **1996**, *53*, 1287–1293.
- [106] C.-J. Lee, A. Mizel, U. Banin, M. L. Cohen, A. P. Alivisatos, *J. Chem. Phys.* **2000**, *113*, 2016–2020.
- [107] K. K. Zhuravlev, J. M. Pietryga, R. K. Sander, R. D. Schaller, *Appl. Phys. Lett.* **2007**, *90*, 043110.
- [108] E. Pedrueza, A. Segura, R. Abargues, J. B. Bailach, J. C. Chervin, J. P. Martínez-Pastor, *Nanotechnology* **2013**, *24*, 205701.
- [109] K. Bian et al., *Phys. Chem. Chem. Phys.* **2014**, *16*, 8515–8520.
- [110] C. D. Grant, J. C. Crowhurst, S. Hamel, A. J. Williamson, N. Zaitseva, *Small* **2008**, *4*, 788–794.
- [111] T. Fischer, S. Stöttinger, G. Hinze, A. Bottin, N. Hu, T. Basché, *Nano Lett.* **2017**, *17*, 1559–1563.
- [112] Y. C. Lin, W. C. Chou, A. S. Susa, S. V. Kershaw, A. L. Rogach, *Nanoscale* **2013**, *5*, 3400–3405.
- [113] X. Yuan et al., *Nat. Commun.* **2018**, *9*, 1–8.
- [114] C. L. Choi, K. J. Koski, S. Sivasankar, A. P. Alivisatos, *Nano Lett.* **2009**, *9*, 3544–3549.
- [115] L. Fang et al., *J. Chem. Phys.* **2007**, *127*, 184704.
- [116] J. Schrier, B. Lee, L.-W. Wang, *J. Nanosci. Nanotechnol.* **2008**, *8*, 1994–1998.
- [117] J. Schroeder, P. D. Persans, *J. Lumin.* **1996**, *70*, 69–84.
- [118] C. L. Choi, K. J. Koski, A. C. K. Olson, A. P. Alivisatos, *Proc. Natl. Acad. Sci. USA* **2010**, *107*, 21306–21310.
- [119] S. N. Raja et al., *Nano Lett.* **2013**, *13*, 3915–3922.
- [120] S. N. Raja et al., *Nano Lett.* **2016**, *16*, 5060–5067.
- [121] B. Zhou, G. Xiao, X. Yang, Q. Li, K. Wang, Y. Wang, *Nanoscale* **2015**, *7*, 8835–8842.

- [122] K. E. Brown, W. L. Shaw, X. Zheng, D. D. Dlott, *Rev. Sci. Instrum.* **2012**, 83, 103901.
- [123] K. E. Brown, Y. Fu, W. L. Shaw, D. D. Dlott, *J. Appl. Phys.* **2012**, 112, 103508.
- [124] W. M. Trott, R. E. Setchell, *AIP Conf. Proc.* **2002**, 620, 1347–1350.
- [125] D. C. Swift, J. G. Niemczura, D. L. Paisley, R. P. Johnson, S.-N. Luo, T. E. Tierney, *Rev. Sci. Instrum.* **2005**, 76, 093907.
- [126] D. L. Paisley, S.-N. Luo, S. R. Greenfield, A. C. Koskelo, *Rev. Sci. Instrum.* **2008**, 79, 023902.
- [127] P. Xiao, et al., *Appl. Phys. Lett.* **2016**, 108, 011908.
- [128] Z. Kang et al., *J. Appl. Phys.* **2016**, 120, 043107.
- [129] J. S. Wittenberg, M. G. Merkle, A. P. Alivisatos, *Phys. Rev. Lett.* **2009**, 103, 125701.
- [130] M. Saliba et al., *Energy Environ. Sci.* **2016**, 9, 1989–1997.
- [131] M. Saliba et al., *Science* **2016**, 354, 206–209.
- [132] X. Zheng, C. Wu, S. K. Jha, Z. Li, K. Zhu, S. Priya, *ACS Energy Lett.* **2016**, 1, 1014–1020.
- [133] M. C. Weidman, A. J. Goodman, W. A. Tisdale, *Chem. Mater.* **2017**, 29, 5019–5030.
- [134] M. C. Weidman, M. Seitz, S. D. Stranks, W. A. Tisdale, *ACS Nano* **2016**, 10, 7830–7839.
- [135] A. Wang, Y. Guo, F. Muhammad, Z. Deng, *Chem. Mater.* **2017**, 29, 6493–6501.
- [136] X. Pang, Y. He, J. Jung, Z. Lin, *Science* **2016**, 353, 1268–1272.
- [137] H. Zhu et al., *Nat. Mater.* **2015**, 14, 636–642.
- [138] M. A. Hines, P. Guyot-Sionnest, *J. Phys. Chem. B* **1998**, 102, 19.
- [139] M. He et al., *Angew. Chem. Int. Ed.* **2016**, 55, 4280–4284; *Angew. Chem.* **2016**, 128, 4352–4356.
- [140] S. Keuleyan, E. Lhuillier, P. Guyot-Sionnest, *J. Am. Chem. Soc.* **2011**, 133, 16422–16424.
- [141] J. Wang, F. Sciarrino, A. Laing, M. G. Thompson, *Nat. Photonics* **2020**, 14, 273–284.
- [142] P. Lodahl, S. Mahmoodian, S. Stobbe, *Rev. Mod. Phys.* **2015**, 87, 347–400.
- [143] C. P. Dietrich, A. Fiore, M. G. Thompson, M. Kamp, S. Höfling, *Laser Photonics Rev.* **2016**, 10, 870–894.
- [144] A. W. Elshaari et al., *Nano Lett.* **2018**, 18, 7969–7976.
- [145] H. M. G. A. Tholen et al., *Phys. Rev. B* **2019**, 99, 1–8.

Manuscript received: June 13, 2020

Accepted manuscript online: July 3, 2020

Version of record online: January 8, 2021